Technische Universität Berlin
School IV - Electrical Engineering and Computer Science
Department of Computer Engineering and Microelectronics
Robotics and Biology Laboratory

Master Thesis

A Tactile Sensor Array for Soft Robotics

presented by

Tessa Johanna Pannen
Matr.-Nr.: 343776
tessa.j.pannen@campus.tu-berlin.de
Computational Engineering Science

Date of submission: **7.10.2020**

Examiners: **Prof. Dr. Oliver Brock, Prof. Dr. Jörg Krüger**
Advisors: **Prof. Dr. Oliver Brock, Steffen Puhlmann**

Declaration

I hereby declare in lieu of an oath that I have produced this work by myself. All used sources are listed in the bibliography and content taken directly or indirectly from other sources is marked as such.

Eidesstattliche Erklärung

Hiermit erkläre ich an Eides statt, dass ich die vorliegende Arbeit selbstständig und eigenhändig sowie ausschließlich unter Verwendung der aufgeführten Quellen und Hilfsmittel angefertigt habe.

Berlin, den

Unterschrift

Abstract

Soft robotics is an emerging field in robotic that develops novel solution in the area of robot safety and robot-human-interaction. Soft robots are build from materials that can passively comply to external forces. This adaptivity allows them to perform robust grasping and manipulation. These soft robots require special sensors that don't restrict their compliance. In this work, we propose a tactile sensor array that can measure pressures on 14 independent taxels. The sensor is made from a piezoresistive fabric layer that enables measuring wide ranges of contact pressures, and the taxels are defined on a custom flexible printed circuit board which allows for a high spatial resolution. We present each step of the design and fabrication process of the proposed sensor. In a sensor characterization we investigate the sensor input-output relation described by a characteristic curve. Under consideration of the sensor influence on the actuator we integrate the proposed sensor into a PneuFlex actuator. A RBO Hand 2 equipped with four tactile sensor arrays grasps a variety of objects. Subsequently we demonstrate the ability of the tactile sensor to perform in-hand object recognition with a SVM classifier.

Zusammenfassung

Titel:
Eine taktile Sensorgruppe für Soft Robotik

Soft Robotics ist ein neues Feld der Robotik welches neue Lösungsansätze für die Robotersicherheit und die Mensch-Maschinen-Interaktion entwicket. Weiche Roboter werden mit Materialien hergestellt die unter äußeren Kräften passiv nachgeben können. Diese Anpassungsfähigkeit ermöglicht es ihnen stabil zuzugreifen und ihre Umgebung zu manipulieren. Diese weichen Roboter benötigen spezielle Sensorik die ihre Nachgiebigkeit nicht beeinflussen. Im Rahmen dieser Arbeit präsentieren wir einen Sensor der auf 14 unabhängigen Taxeln Druck messen kann. Der Sensor ist aus einem piezoresistiven Stoff gefertigt und kann dadurch in einem großen Messbereich Berührungsdruck wahrnehmen. Die Taxel sind durch eine maßgefertigte flexible Leiterplatte voneinander abgegrenzt was eine hohe räumliche Auflösung ermöglicht. Wir legen die einzelnen Schritte der Sensorentwicklung und -herstellung dar. In einer Sensorcharakterisierung untersuchen wir dann das Verhältnis zwischen Sensorein- und ausgang welches die Kennlinie des Sensors beschreibt. Unter Berücksichtigung des Einflusses des Sensors auf den Aktuator und umgekehrt intergrieren wir den Sensor in einen PneuFlex-Aktuator Mit einer RBO Hand 2, welche mit 4 Taktilen Sensorgruppen ausgestattet ist, greifen wir eine Vielzahl an Objekten. Anschließend demonstrieren wir mit einem SVN-Klassificator die Fähigkeit des Sensors, die Objekte durch Greifen zu erkennen.

Contents

List of Figures

List of Tables

Notation Remarks

The following notational conventions are used throughout this thesis:

- Scalars are shown in lower case / upper case mixed: s, S
- Vectors are shown in lower case bold: $\mathbf{v}$
- Matrices are shown in upper case bold: $\mathbf{M}$
- Generalized inverse matrices are marked with a #: $\mathbf{M}^{\#}$
- Homogeneous Transformations from frame A to frame B are shown as: ${}^{A}_{B}\mathbf{T}$
- Priorities of feedback control behaviors are indicated as ascending from left to right: $\phi_{\text{low}} \lhd \phi_{\text{high}}$
- Non trivial function names are written in upper case: FUNCTION
- Trivial function names (getter and setters) are written in lower case: function
- Complex entities (robot model, map, observations) are marked in blackboard bold: $\mathbb{R}$

1 Introduction

Soft Robotics is generally speaking the field of robotics that explores the design, manufacturing, control and usage of robots that were build from soft materials. A sub-field of soft robotics is devoted to soft robotic hands. During interactions with their surrounding, soft hands can deform and comply to their environment.
When grasping an object, the morphology of the soft gripper passively adapts to the object. This so called morphological computation compensates uncertainties in sensing and actuation and helps the hand to create a stable grasp. It can thereby take over the small corrections and adjustments that are necessary for robust grasping. Because these adaptations occur passively, little information are available about the internal processes of the actuator. Sensory feedback is therefore essential to further improve grasping or learn more about the interaction of the hand with its environment.
The softness of the hand poses a challenge when we add sensors. Standard sensors are rigid and would change the compliant behavior of the soft actuator. To keep the advantage of the soft material, we have to make sure that additional sensors don't restrict the movement of the soft gripper. For soft robotic hands we need to develop special soft and flexible sensors.

We desire sensory feedback to better understand and control the interaction of the gripper with its surrounding. One way to learn about the environment is by observing the contact of the hand during an interaction. This contact can occur between a soft gripper and itself, a fixed environment such as tables, boxes or walls, and loose object that can be grasped, shuffled, lifted and placed. Tactile sensors can deliver a variety of contact information, such as temperature, proximity, vibration, contact pattern, pressures, forces, or shearforces. We can draw information about surface structures from vibrations [1] and contact pattern [2]. Proximity can tell us about the relative position of the gripper to its surrounding [3], while force and pressure data can help distinguish grasped objects of different weighs or shapes [4][5].

To provide tactile feedback to a soft robot hands, we propose a novel flexible tactile sensor array. It can measure a range of contact pressures across an array of independent tactile pixels, or taxels for short. By looking at related work, we find and combine the most promising technologies to create the sensor. We then investigate

the abilities of the sensor based on its characteristic curve that defines the relationship between the sensory in- and output.
The sensor array is then deployed on a PneuFlex actuator [6], a soft pneumatic actuator. Merged to each other, we investigate the effect of the actuator and the sensor on each other; How the actuator movement influences the sensor output, and how the addition of a sensor influences the compliance of the actuator.
Finally a RBO Hand 2, a soft anthropomorphic hand made of PneuFlex actuator, is sensorized with the proposed sensor. By grasping nine different objects we show the ability of the tactile sensor to classify objects based on their contact information. In comparison to the air pressure measurements provided by the air compartments of the actuators we demonstrate how the sensor can significantly improve the in-hand recognition rate of a soft hand. In this scope we confirm the contribution of the high taxel resolution to the outstanding classification of the tactile sensor array.

A possible sensor design needs to fulfill a set of requirements:
The compliant behavior of the actuator must not be restricted by the sensor. Therefore, the final sensor and each material used in the sensor needs to be *thin and flexible*. The contact of the actuator with it's environment can occur in different locations on the actuator and the contact pressure can have different intensities. To distinguish these contact patterns, the sensor array requires a *high spatial resolution*. To achieve this, the taxels need to be clearly separated from each other. Furthermore wiring has to access the information of all taxels without interfering with the sensor readings, not restrict the workspace of the actuator, and avoid cross-talking among taxels [7]. The complexity of the wiring problem rises with the spatial resolution [7]. Additionally, to detect subtle differences in contact patterns, each taxel of the sensor should have a *high sensitivity* to small changes in pressure and can output them in continuous readings. It is also desirable if each taxel can produce a useful sensor output for a *large range* of pressures. Yet we have to be aware that the dynamic range of a tactile sensor decreases with increasing sensitivity, as these two properties are contradicting each other due to technology restrictions[7].
A look at recent research in the following chapter will give an overview over the available materials and technologies to satisfy these requirements.

2 Related Work

Existing soft tactile sensors use different physical effects, mainly capacitive, piezoresistive or resistive [8][9][10]. They have been used in various configurations by different researchers.
Capacitive tactile sensors, at their core, have two conductive layers seperated by a permittivity dielectric. The capacity C depends on the area size A, the permittivity of the dielectric ϵ_r and vacuum ϵ_0, and the thickness of the dielectric d: $C = \epsilon_0 \epsilon_r \frac{A}{d}$.
Soft capacitive sensors use soft materials to create the conductive and dielectric layers. Upon a contact pressure, the dielectric is compressed (d decreases), and as a result the capacity increases measurably . Therefore, a thick dielectic with high compression rate make a sensor with large measuring range [4].
[4] created a capacitive sensor with a single oval taxel based on this method. Their dielectricum layer, made from silicon, is ≈1mm thick and contains micropores to increase the compression rate. Attatched to the thumb of a wearable glove, the sensor can distinguish between grasped objects of different weight [4]. Since the capacity depends on the sensing area of the sensor, the size can non be scaled down without compromising the quality of the sensory output.
[3] used the capacitive effect to develop a proximity sensor. It has only one conductive fabric layer, the environment serves as second conductive surface and the air gap as dielectric. [3] uses an etching solution on the conductive fabric to define 8 independent taxel along the sensor surface. Metal wires are stitched onto the backside of each taxel to connect them to a wire bus. This etching method creates clearly defined taxel borders even if the taxel are less than 3mm apart [3], and could possibly be used to create an even higher spatial resolution. The cabling solution even increases the proximity detection [3], but creates a elevation in the middle of each taxel. This is undesirable for contact pressure sensing because an uneven sensing surface means that the contact pressure is distributed unevenly and can pollute the sensor readings.

Another approach to tactile sensing is the resistive or piezoresistive effect. So called force-sensing resistors (FSR) change their electrical resistance when a force or pressure is applied.
Liquid metals are known for changing their resistive properties under deformation. EGaIn filled microchannels, arranged in a spiral pattern in an elastomer, can measure strain and pressure [11]. Integrated in the fingertip of a pneumatic actuator,

this sensor can be used to control applied pressure [12] or the stiffness [13] of the actuator. The total length of the microchannel is crucial for the functionality of the sensor [11], therefore the taxel size can not be scaled down to fit multiple smaller taxels on the same area.

Elastomers can be given piezoresistive properties by mixing in carbon black particles [14][15]. The elastomer deform under contact pressure and in this process changes its resistivity. [14] places a strip of resistive elastomer vertically inside a silicon cylinder of 20mm height. Under a load of 3N, the resistance of the strip increases by 8%. The vertical positioning is space-efficient, and could allow a high resolution of multiple sensing stips. If a soft actuator is approximately modelled after a human finger, such a sensing bud of 20mm height would be thicker than the actuator itself. Therefore, the sensor would change the shape and probably the morphology of the actuator, which we intend to avoid. [15] placed a layer of such a piezoresistive elastomer between two conductive fabric sheets. Cutting these sheets into stripes created a grid pattern of large tactile cells. As tactile skin, it can cover industrial robots to increase safety during human-robot-interactions [15].

A thinner alternative to carbon black elastomers is Velostat™, a flexible polyolefin foil infused with carbon black that is produced by 3M (US-MN). It is only 0.1mm thick and has a volume resistivity of $<5\Omega$-m[1] that can drop by up to 80% under a load of 20N [16]. [17] used Velostat to develop a tactile sensor array with five independent taxel. The taxels are read with conductive thread that is placed on each taxel. This sensor has been shown to allow force-feedback control and haptic perception based on contact pattern and pressure [17]. Due to it's thinness, the compression rate an therefore the measurement range of Velostat is limited, but it is still able to provide continuous sensor outputs.

Its measurement range is surpassed by EeonTex™ LTT-SLPA, a conductive stretchable fabric produced by Eeonyx (US-CA). It has a volume resistivity of $\approx$20kΩ-m [18] that drops by up to 99% under compression [18]. The nylon fibers of the fabric are coated with carbon, and the fabric is only 0.38mm thick[2]. [19] created a tactile sensor with only one 2cm$\times$2cm taxel, Where the EeonTex is placed between two conductive layers. They each have fabric overhang on the side of the sensor where the cables to read the sensor are soldered on. [19] applied the sensor to the fingertip soft robotic actuators for closed-loop force control. [20] equipped the fingers of a pneumatic actuator with seven of these taxels. As a result, the cables of each taxel stick out the side of the finger. These cables can get entangled and ripped out during

[1] According to data sheet

[2] According to data sheet `http://www.eeonyx.com/`

interactions with the environment Yet, with their tactile sensor array [20] can infer the force distribution along the actuator while grasping different objects. On a larger scale, [21] developed an EeonTex-based shoe insole for gait analysis. They achieved a resolution of 36 taxels with contact pads on a flexible printed circuit board (flexPCB). Two of these flexPCBs are placed facing each other with the EeonTax layer in between. The sensor reading can be read from small copper outputs on the side of the flexPCB, from where flat conductive line connect them to each taxel. This method has the advantage that the cabling of each taxel is moved away from the contact surface onto the edge of the flexPCB. In this setup, the flexPCB is the most rigid component. Since one flexPCB is sufficient to read the sensor data from our tactile sensor array, we could replace one flexPCB with a soft conductive fabric to increase the flexibility of our sensor.

For the sake of completeness we also include commercial suppliers that can already provide a wide range of tactile sensor arrays. CMV Hoven GmbH (GER), offers thin film sensors made from plastic sheets, available in sizes between 3mm and 1768mm on each side and resolutions of up to 248 taxels/cm^2. As the unique shape of most soft actuators require a custom sensor shape, sensors from this supplier cost ∼30-40k€[3].
Pressure Profile Systems, Inc. (UK) offers a flexible pressure sensors which is around 1mm thick and can adjust to curvature and movement of an actuator. The sensing elements can be between 2mm×2mm and 10mm×10mm, the sensing area is available in custom size ranges. A custom shaped sensor array from this supplier costs ∼10k€[4].
Self-build sensors can therefore be an affordable alternative to commercial solutions.

[3]cost estimate by supplier CMV Hoven GmbH, DE https://www.cmv.de/en/ , on July 1st 2020
[4]cost estimate by supplier PPS, UK https://pressureprofile.com/ , on May 15th 2020

3 Tactile Sensor Array

3.1 Sensor Design

3.1.1 Design, Materials and Fabrication

The tactile sensor array we propose is made from three layers. EeonTex™ LTT-SLPA piezoresistve fabric is placed between a layer of Medtex P130 conductive fabric and a custom printed flexible PCB (flexPCB). The property of the EeonTex to drop its electrical resistance under compression enables the sensor to detect contact pressure.
The custom flexPCB carries conductive copper electrodes that form the distinct taxels of the sensor as visualized in Fig. 3.1. Taking inspiration from the human hand where the highest density of tactile cells are located in the finger tip [23], the flexPCB displays nine smaller 3mm×3mm taxels at the side of the sensor that will be attached to the finger tip of the actuator. Six larger 3mm×13mm taxels cover the remaining length of the actuator finger. The outputs of all taxels are located at the base of the finger, here the cables are soldered to the flexPCB. This way, the cables are kept out of the working space of the actuator.
The Medtex P130 is the grounding of the sensor.

These three layers need to be connected to each other by an adhesive to keep the sensor together. Therefore we require two adhesive layers, one between the

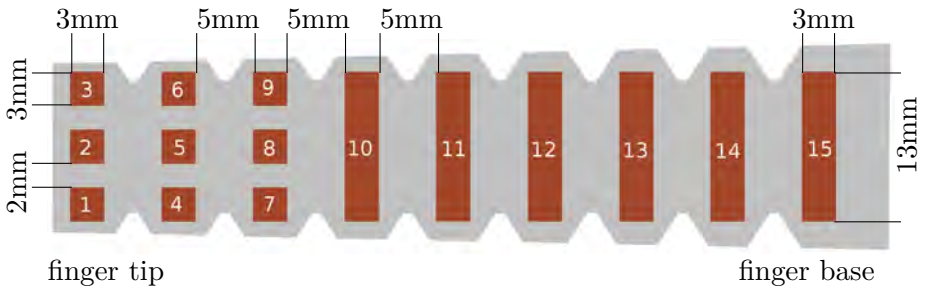

Figure 3.1: The distribution of taxels on the flexible PCB provides a higher density of taxels at the finger tip of the actuator and a lower density along the length of the actuator. This mimics the human hand, where the highest concentration of tactile sensing cells are located in the finger tip [22].

Table 3.1: Overview of all tested adhesives to join the three sensor layers, and how they were applied. The graphics in the right column show the distribution of the adhesive relative to the flexPCB, but the same pattern was used twice, once between flexPCB and piezoresistive fabric, and one between the piezoresistive and conductive fabric layers.

Adhesive	Covered Area
Super Glue: The glue is evenly distributed on the non-conducting surface of the flexPCB	
Super glue: Small dots of superglue equally distributed on not-sensing surface, taxel areas are spared	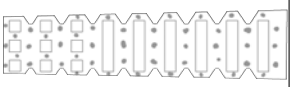
Conductive glue: The liquid glue is spread only on the sensing taxel area with the help of a needle tip	
M3 adhesive tape Due to its anisotropic properties, the adhesive is applied to the whole surface of the flexPCB	
Double-sided adhesive tape: Cut with a laser cutter, the tape covers all non sensing areas. The taxel are cut out.	

flexPCB and the piezoresistive fabric, and one between the piezoresistive and the conductive fabric. The adhesive must not alter the conductive properties of the flexPCB, EeonTex, or the Medtex. Furthermore, the adhesive has to be thin and flexible like all other components of the sensor. We tested several types of adhesive, both solids and liquids as well as conductive and non-conductive:

- Super Glue is a quickly drying liquid and once dry does not conduct electricity[1].
- Coductive Glue is a liquid adhesive the contains small silver particles to make it electrically conductive even in cured state. It is commonly used to fix broken solder joints.
- Doublesided Adhesive Tape is common stationary supply. It has insulating properties[2] and can stick to almost any even surface.
- M3 Conductive Adhesive Tape is a double sided transfer tape that contains small silver particles and was developed to bond to PCBs and flexPCBs. It allows anisotropic conductivity only through the adhesive thickness, but not sideways.

With each adhesive we be build a sensor array, with super glue we built two sensors to test two different glue patterns. Table 3.1 describes in more detail how these different adhesives are applied to the sensor. Then we test with an ohmmeter how the taxels of each sensor respond to pressure. If the glue does not change the conductive behavior of the sensor layers, the taxels show always the same resistivity when there is no pressure, and the resistivity should drop when we press down on the taxel. When the pressure is removed again, the resistivity should return to its previous state.

Trying the different adhesives led to the following insights:
Both sensors build with super glue show the same behavior. Most taxels have a reproduceable sensor reply where applying pressure causes a resistivity drop, and removing the pressure makes the taxel reliably return to the previous constant resistivity. On both sensors more than 20% of the taxels have a 'jumping' sensor response, where during the unloaded state the resistivity jumps between seemingly random values that are between 50% and 80% of the resistivity of the stable taxels. The reason for this behaviour could be that the fabric layers of the sensor soak in

[1]Tested with ohmmeter
[2]Tested with ohmmeter

the liquid adhesive. If the adhesive creeps to where the taxels are located, it changes their resistive properties. To avoid this effect, we also tested the application of a primer to the fabric before using the super glue. The super glue reacts in contact with the primer, cures faster and therefore has less time to settle into the fabric. Unfortunately the primer causes the super glue to become stiff and brittle during the accelerated curing process, while the sensor behaviour does not improve. It did therefore not improve the results.
The sensor build with conductive glue falls apart easily, as its adhesive power is too low to hold the layers together. Without load, half of the taxel show a resistance of 120-230Ω and a drop of resistance of up to 50Ω under load. These values are only a fraction of the resistance of the EeonTex fabric. The other half of the taxel has a constantly resistance of less than 50Ω unregarded of the load. Here, the glue was applied directly to the locations of the taxels and, similar to the super glue, the adhesive soaked into the fabric layers ans altered their conductive properties.
To build a sensor with double-sided adhesive tape as connecting layers, we fist have to cut out the area of the taxels to allow electrical current to flow through. We cut out the taxel shapes using a laser cutter which guarantees precise and clean cut edges. The sensor build with this tape shows constant resistance when no pressure is applied, a drop in resistance under load and a reliable return to the previous constant resistance when the load is removed.
When the M3 conductive adhesive tape is used to connect the layers of the tactile sensor array, it can cover the whole sensor surface because it is conductive only through its thickness. It can therefore not cause cross-taking of the taxels. When used to build a sensor, each taxel shows infinitely high resistance, unregarded of the applied pressure. Even though the adhesive of the tape bonds the layers strongly together, the conductive silver particles in the tape seem unable to connect to the rougher textile surfaces of the fabrics in order to transmit any electrical current.

In conclusion, the double-sided adhesive tape gave the most stable results. The final composition of the sensor, it is made from five layers in total: The flexPCB, the piezoresistive EeonTex, the conductive Medtex and two layers of double-sided adhesice tape. In preparation of the assembly, the tape is cut with a laser cutter to fit the shape of the flexPCB and with holes in the places of the copper electrodes. In Fig. 3.2 the separate layers are pictured in the order of assembly, with the first layer at the bottom. The steps to build a tactile sensor array are the following:

1. Place a flexPCB on a even surface and make sure the copper electrodes are clean from dust and oil.

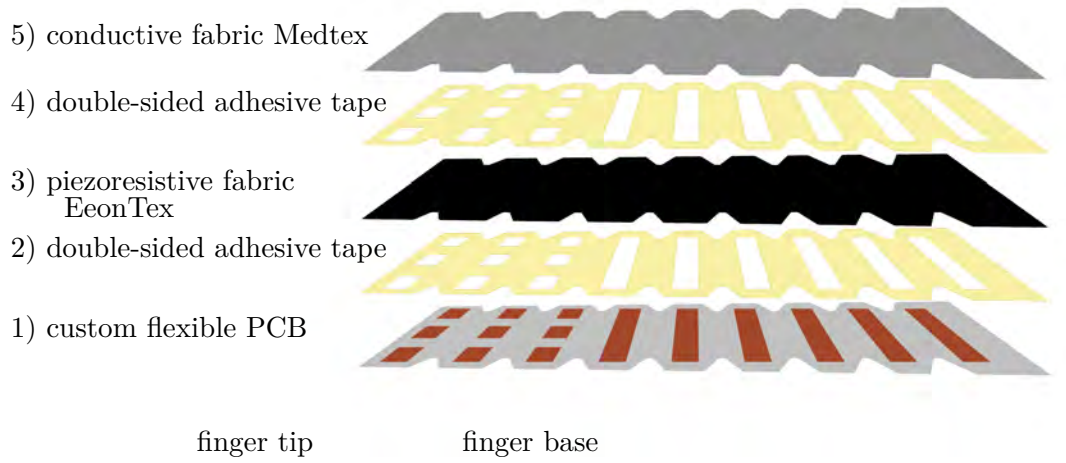

Figure 3.2: The tactile sensor array is made from three layers plus two adhesive layers.

2. Place a laser-cut adhesive tape on the flexPCB. The holes in the adhesive tape leave the taxels free and the border of the tape aligns with the outlines of the flexPCB. Press the adhesive on and peel off the carrier tape.

3. Place a layer of EeonTex piezoresistive fabric on top of the adhesive and press it on. The fabric must cover the whole sensor. With a pair of scissors, cut along the outline of the flexPCB and remove all overhanging fabric.

4. Place the second laser-cut adhesive tape on the EeonTex fabric. The border of the tape aligns with the outlines of the flexPCB. If this step is executed with diligence, the holes in the adhesive tape will be automatically aligned with the electrodes of the flexPCB below. Press the adhesive on and peel off the carrier tape.

5. As final layer, place the conductive Medtex fabric on the adhesive tape and press it on. The fabric must cover the whole sensor. With a pair of scissors, cut along the outline of the sensor and remove all overhanging fabric except for a fabric overhang at the short sensor end that faces the finger base.

6. Solder the 14 cables for the 14 taxel to the output of the flexPCB. Attach one additional cable to the fabric overhang of the conductive layer, this is the grounding of the sensor.

Figure 3.3: The proposed tactile sensor array as finished product

The finished sensor is depicted in Fig. 3.3. A more in-depth construction manual with lists of all required materials and tools can be found in Appendix A.

In this scope we also considered cutting the Medtex and Eeonyx fabric with a lasercutter. Since the fabrics are both made from knitted nylon, they are suitable for laser cutting. The advantage of cutting nylon fabric with laser is that the heat of the laser seals the seams of the fabric while cutting it and produce clean edges. In a compatibility test, we burned samples of both fabrics with a common lighter. Both fabrics produced a stench and the heat causes a change of color in proximity of the burned edges. Since not all chemical components of the fabrics are known, we can not rule out that the burning releases harmful toxins. For this reason, we abstained from the laser cutting and instead cut both fabrics with scissors.

3.1.2 Reading Setup

The proposed sensor based on Eeontex fabric exploits the conductive property of the material. In a relaxed, unloaded state the piezoresistive fabric has a volume resistivity of ≈20kΩ-m. When an applied pressure compresses the fabric, this resistivity drops by up to 99% [18]. The bigger the load on the fabric, the lower the resistance [3].

To read a signal from the sensor array, we need to measure this change of resistance of each individual taxel R_{taxel}. Therefore we connect one taxel R_{taxel} in series with a known resistor R_{pullup}, and apply an input voltage U_{source} across both. The voltage divider equation states that voltage and resistance of the taxel are now proportional

[3] correlation confirmed with an ohmmeter

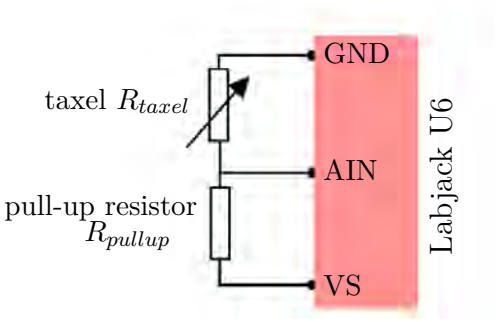

Figure 3.4: The schematic diagram shows the circutery to read the signal from a single taxel. R_{pullup} is a resistor with a fixed value. The taxel that changes its resistance depending on the load applied to it is represented by a variable resistor R_{taxel}. R_{pullup} and R_{taxel} are connected in series. The voltage source (VS) connected to the pull-up resistor is $U_{source} = 5V$, while the sensor is connected to the ground (GND). In between, we can measure the output voltage of the taxel U_{taxel} at the Analog Input (AIN) of the Labjack U6. For each taxel of a tactile sensor array, such a voltage divider setup is necessary.

to the input voltage and the sum of all resistors:

$$\frac{U_{taxel}}{U_{input}} = \frac{R_{taxel}}{R_{taxel} + R_{pullup}} \tag{3.1}$$

Solved for the output voltage U_{taxel} we get a measurable value that changes proportionally with the change of the taxel resistivity R_{taxel}:

$$U_{taxel} = \frac{R_{taxel}}{R_{taxel} + R_{pullup}} * U_{source} \tag{3.2}$$

Fig. 3.4 shows the electrical circuit diagram of such a voltage divider. The taxel R_{taxel} is represented by a variable resistor that changes upon pressure[8]. Because U_{source} and R_{pullup} remain constant values, the change of U_{taxel} depends solely on R_{taxel}. At the output U_{taxel} we measure a voltage that is proportional to the resistance of the taxel R_{taxel}.

The output Voltage U_{taxel} is read by a Labjack U6, a data acquisition (DAQ) device. The Labjack U6 also provides the voltage source (VS) U_{source} and the grounding GND. Since the Labjack U6 connects to the computer via USB, it can provide the maximal supply of $U_{source} = 5V$.
With a DB37 connector, the Labjack U6 reads up to 14 analog signals. The spatial resolution on the flexPCB has a total of 15 taxels, 9 small taxels at the finger tip and 6 larger taxels along the length of the finger, see Fig. 3.1. To read the values

of each taxel, we need a total of 15 voltage dividers and two Labjack U6. In the future we aim to fit multiple tactile sensor arrays to a soft hand. The space around a gripper to place Labjack U6 data acquisition boxes and breadboard for voltage dividers is limited and could lead to logistical problems in future experimental set-ups. Efficient data acquisition with best use of space is therefore of interest.
With this constraint in mind we decided too use only one Labjack U6 per sensor array. This allows to read 14 taxel values. The large taxel that is closest to the finger base will not be connected to the data acquisition. In Fig. 3.1, this corresponds to taxel number 15 on the far right side. We decided to leave out taxel 15 to maintain the equal spacing among the remaining taxels.
The voltage dividers are realized on a plug-in breadboard. In this set-up, we use pull-up resistors with $R_{pullup} = 4.7k\Omega$. We found this value by trying resistors of different orders of magnitude. With $R_{pullup} = 4.7k\Omega$ produce a fast sensor response under a increasing pressure. The pull-up resistor is just an temporary value, and we will explore other pull-up resistors and their influence on the sensor sensibility in Sec. 3.2.2.

3.2 Sensor Evaluation

3.2.1 Characteristic Line

The change of resistance inside each taxel can be measured via the voltage divider as described in the previous chapter, but a user can not intuitively interpret a voltage value as a measurement for contact pressure. Therefore we need a method to translate the voltage to a pressure value. The characteristic line or characteristic curve of a sensor is a graph that gives the relationship between the input and the output of the sensor. In our case the contact pressure is the input, and the voltage U_{taxel} is the output. The contact pressure p depends on two independent variables, the applied force F and the contact area A:

$$p = \frac{F}{A} \tag{3.3}$$

If both force and contact pressure are known, we can compute the contact pressure. For the the same contact pressures our sensor will always produce the same sensor outputs. The relationship between the loaded pressure and the sensor output form the characteristic line of our sensor.

To find this relationship we use differently sized probe tips to apply force to the

tactile sensor. This way we ensure that the characteristic line is valid for every contact area. The applied force F during a loading process and the resulting sensor response U_{taxel} are recorded. Since the probe tip areas are known, all force values can be normalized to pressure values using Eq. 3.3. If the relationship between the contact pressure and the sensor response can indeed be described with equation 3.3, all measurement series fall on one common characteristic line.

Seven different probe tips are used for the measurement, they are circular with diameters of $d \in [4, 6, 8, 10, 12, 14, 16]mm$. These probe tips are laser cut from acrylic glass to ensure flat surfaces and clean edges. Since the probe tips we test are larger than the big taxels on the proposed sensor, we use a special sensor patch. The test patch has the same layered structure as the sensor array, the only difference is the flexPCB. Where on the proposed sensor the taxels are defined by the separate copper electrodes, we now have one continuous copper surface that form a single large taxel. This allows us to try a larger range of probe tip sizes without worrying that the probe tip exceeds the taxel boundaries. We can read the sensor response U_{taxel} of this tactile sensor patch via a voltage divider and a Labjack U6 as descriped in Sec. 3.1.2.
To measure the applied force F we use a force torque sensor (F/T sensor). It is mounted to a vertical guiding rail, with the tool adaptor plate facing downwards. Attached to the tool adaptor plate is a screw with a flat screw head. An acrylic tray on the ground provides a smooth underground surface. The setup is depicted in Fig. 3.5. When the F/T sensor is pushed downwards along the rail, it presses down with the screw head pointing down. When the screw head touches a surface, the F/T sensor measures the forces the screw head applies to said surface. From the F/T sensor we can acquire forces and torques from all three cartesian coordinates. The screw on the tool adaptor plate is placed at the origin of the reference frame of the sensor and points in the z-axis which is orthogonal to the tool adaptor plate. Therefore we need only the z-component of the force to get the force applied by the screw head.

When we record a loading process on the tactile sensor, each recording containing 70 data pairs of applied force F and the corresponding sensor response U_{taxel}. To record a data row, we place the tactile sensor patch on the acrylic tray under the force torque sensor. A probe tip is placed on top of the tactile sensor and under the screw head mounted to the F/T sensor. At the beginning of the recording, the screw head hovers over the tactile sensor, not applying any pressure. Then we record measure 70 data pairs as we manually push the F/T sensor down. The screw

Figure 3.5: In this setup the force torque sensor is attached to a vertical rail with the help of a orthogonal connecting link made from acrylic glass. On its tool adaptor plate we attached a screw with the screw head pointing down. On this rail, the sensor can be moved up an down and the screw can apply and measure a force downwards. Below is a tray made from acrylic glass with several rows of elastic straps. The tray provides a smooth underground to place the tactile sensor on while the elastics hold it in place.

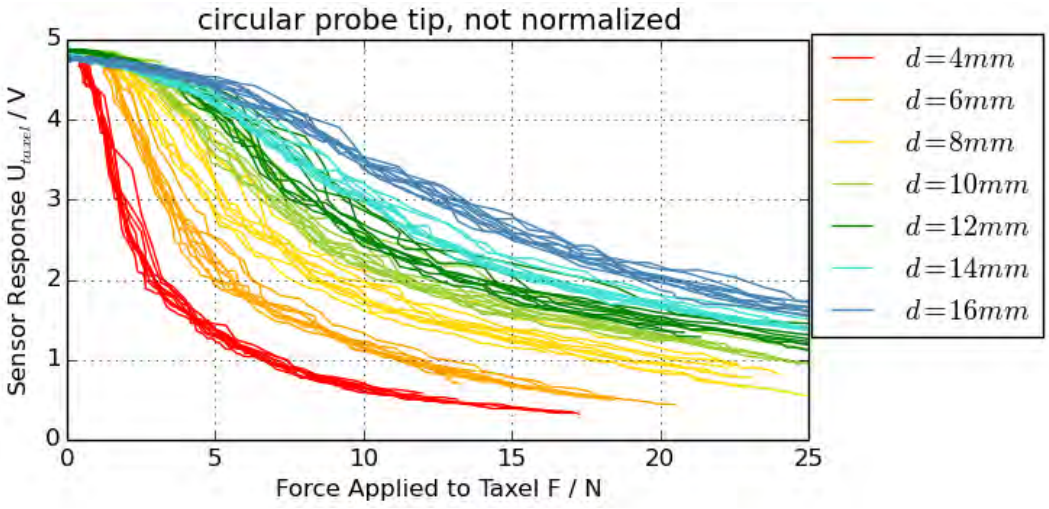

Figure 3.6: The graph shows the sensor response to a loading processes. As the force pressing on the sensor increases, the sensor response U_{taxel} decreases. The bigger the probe tip, the slower the sensor answer decreases.

head presses on the probe tip which again distributes the force equally on its surface and presses on the tactile sensor. For each of the seven probe tip sizes, the loading process is recorded 10 times, resulting in in a total of 70 recorded loading processes.

The applied forces and their corresponding sensor responses for the different probe tip sizes are shown in Fig. 3.6, each color represents one probe tip size. All data of the same probe tip size lie on a common line with a inverse sigmoid looking shape. For small pressures, where all measurements show almost $U_{taxel} = 5V$, these lines are flat, followed by a steeper slope that flattens out when it converges towards $U_{taxel} = 0V$. The bigger probe tips result in a smaller slope in the sensor reaction. This is aligned with the knowledge that the same force is distributed on a bigger area, which results in a smaller contact pressure that can therefore cause less compression in the piezoresistive layer of the sensor.

Next, we normalize the force values on the x-axis of Fig 3.6 to pressure value. For each loading process, we compute the pressure by dividing the force by the area of the probe tip that was used (Eq. 3.3). The area A_{circle} for each circular probe tip is computed based on its diameter d:

$$A_{circle} = \pi \left(\frac{d}{2}\right)^2 \tag{3.4}$$

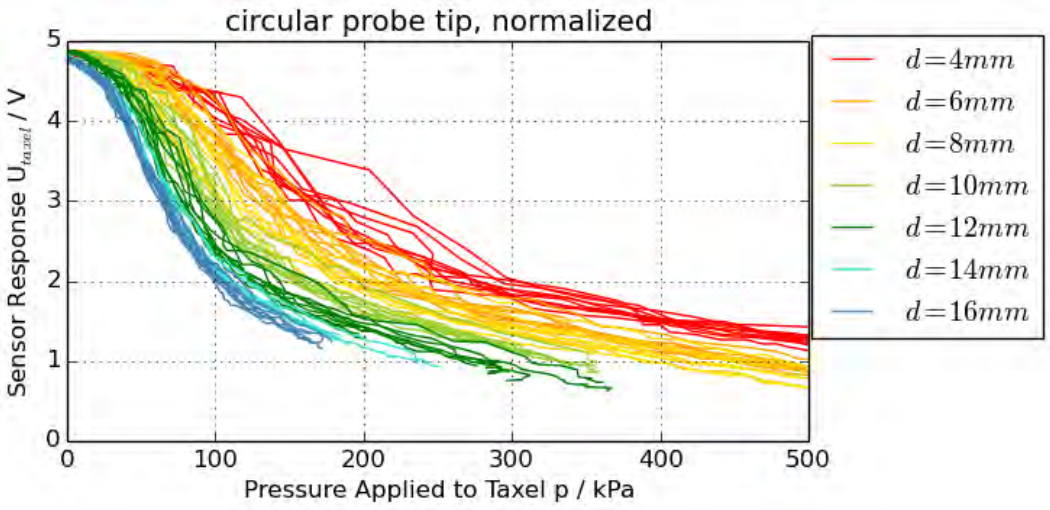

Figure 3.7: The graph shows the same sensor response to a loading processes. The applied force on the the x-axis is normalized to a pressure value using the known probe tip area.

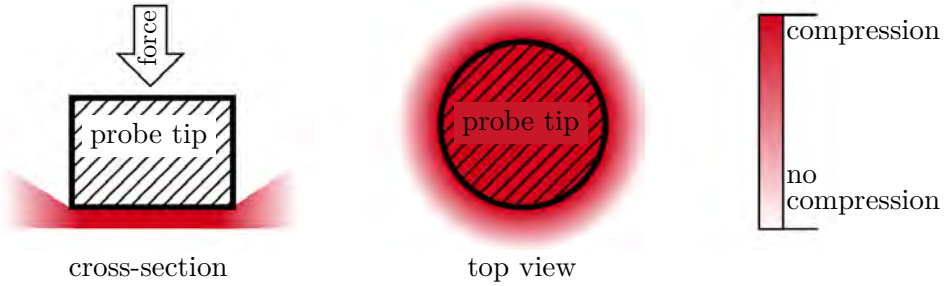

Figure 3.8: When the piezoresistive fabric is compressed, the area around the probe tip only relaxes gradually and adds to the conductivity of the fabric (cross-section on the left). In case of a round probe tip, this increases the area of compression by a ring around the probe tip (top view on the right).

The normalized graphs are shown in Fig 3.7. Compared to figure 3.6, the order of the probe tip sizes is inverted, the larger the probe tip the steeper the slope of the lines.

Unlike expected, the data points do not converge to a single characteristic line. This suggests that the normalization by the probe tip area is not sufficient to map the force to a pressure.

Until now the compression mechanics of the piezoresistive fabic, which is an elastic material, was not considered. As the fabric right under the probe tip is compressed, there has to be an area around the probe tip in which the compression gradually decreases. This partially compressed fabric adds to the area in which the conductivity of the fabric is increased. Therefore, the area of compression is larger than

the probe tip area. This effect is visualized in Fig. 3.8.
Applied to the loading processes of Fig. 3.6, we now use the area of compression instead of the probe tip area to normalize the force values. With this improved normalization, all data should fall together and form the characteristic line.

To ensure that the compression area enables the mapping from force to pressure, we test this solution for other contact shapes beside the round probe tips. For this reason the force and sensor response of a loading process are recorded again, this time with square probe tips. We extend the probe tip area (Eq. 3.4) by the area of gradual decompression. As simple model, we describe the area of compression around the probe tip by dilating its shape by a disk with radius x. This is a approximation, because the actual slope of the decompression around the probe tip is unknown.
The last step is finding the best dilation radius x to represent this area of compression. When we map the loading forces to pressure values, all loading processes should converge closer together. Then we use the area of compression of both probe tip shapes to normalize the corresponding loading processes. As a score for how well all loading processes converge we compute the standard deviation of the sensor response U_{taxel} along the x-axis. With systematic testing we optimize the dilation radius x for the standard deviation, separately for the circular and the square probe tip. We can then compare the dilation radius for both probe tip shapes and the characteristic line they produce.

For the new loading processes we use square probe tips with edge length of $l \in [3.55, 5.35, 7.09, 8.86, 10.63, 12.41, 14.18]mm$. These side length were specifically chosen because they produce the same area sizes as the previously used round probe tips with diameter $d \in [4, 6, 8, 10, 12, 14, 16]mm$. The recording process with the square probe tips is identical to the round probe tips. Like before, 10 loading processes are recorded for each probe tip size as shown in Fig. 3.9.
The area of compression of each probe tip is computed by dilating the area a disk with radius x. This radius is a fixed value, which means that the dilation width remains the same regardless of the probe tip size. Fig. 3.10 shows the dilation for both the circular and the square probe tip. For a circular probe with diameter d we get a compression area $A_{comp.circle}$ of:

$$A_{comp.circle} = \pi \left(\frac{d}{2} + x \right)^2 \tag{3.5}$$

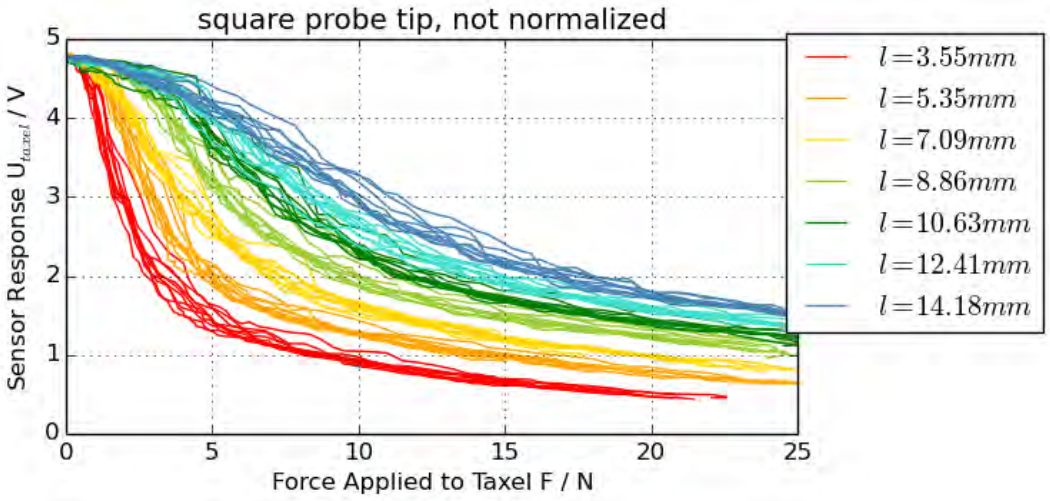

Figure 3.9: The graph shows the sensor response to a loading processes with square probe tips. As the force pressing on the sensor increases, the sensor answer U_{taxel} decreases.

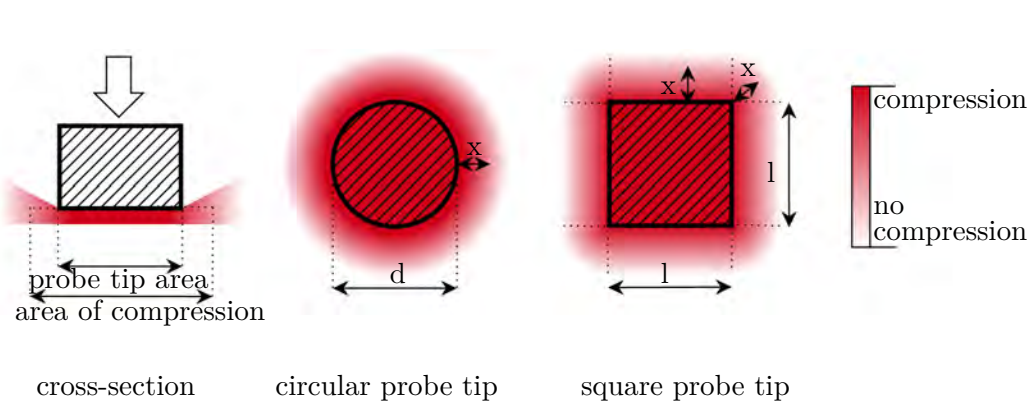

Figure 3.10: The actual slope of the decompression around the probe tip is unknown (right). We therefore approximate it with a dilation by a radius x. For the circular probe tip (center) with diameter d, the compression area is circular as well but with a new diameter that is $d + 2x$. To compute the compression area of the square probe tip (left) with edge length l, we add four rectangles of size lx on each edge and four quatercircles with radius x at the corners.

The compression area $A_{comp.square}$ of the square probe tip of edge length l becomes:

$$A_{comp.square} = \underbrace{l^2}_{\text{probe tip area square}} + \underbrace{4lx}_{\text{four dilated sides}} + \underbrace{4\frac{1}{4}\pi x^2}_{\text{four dilated corners}} \tag{3.6}$$

$$A_{comp.square} = l^2 + 4lx + \pi x^2 \tag{3.7}$$

In order to use these two areas in Eq. 3.3 to map the force to pressure values a value for the dilation radius x needs to be found.

The best value for the dilation radius x will converge all loading processes on a common line. We search for the best radii independently for each probe tip shape, x_{circle} and x_{square}, because this will later allow to compare them to each other. We insert radii between $x = 0.0mm$ and $x = 3.4mm$, in steps of $0.2mm$, to Eqs. 3.5 and 3.7 in order to compute the compression areas. With the compression areas we normalize the force values on the x-axis of Figs. 3.6 and 3.9 by using Eq. 3.3.
To score how well the data converges, all the normalized pressure values along the x-axis is discretized in steps of 5kPa. For each discrete step we compute the average and standard deviation of the sensor response U_{taxel}. The highest found standard deviation becomes the score for the used dilation radius x. The smaller the score for a dilation radius, the better the lines of the loading processes converge.

All computed standard deviations for the tested radii x are shown in Fig. 3.11. Overall the loading processes that were recorded with the square probe tips converge better than the circular probe tips, as they reach smaller standard deviations for every tested radius. On the left of the top graph, for dilation $x = 0$, we reach the biggest standard deviations. This corresponds to the first normalization attempt where we only used the probe tip area, see Fig. 3.7. In Fig. 3.11 we find the smallest standard deviations for the circular and the square probe tip, which are for the dilation radii $x_{circle} = 2.2mm$ and $x_{square} = 2.1mm$. A refined search with smaller step sizes of $0.01mm$ for these radii values, shown in the bottom of Fig 3.11, delivers $x_{circl}e = 2.21mm$ and $x_{square} = 2.11mm$.

The dilation radius x was introduced as an approximation for the decreasing compression around the probe tip. These two found radii values lie close together and in their close proximity the standard deviation that we used to score the radii fluctuates, likely due to measurement noises. In most applications of the tactile sensor the exact shape of the contact is unknown. For this reason the dilation radius should be independent from the contact shape. We therefore choose a universal

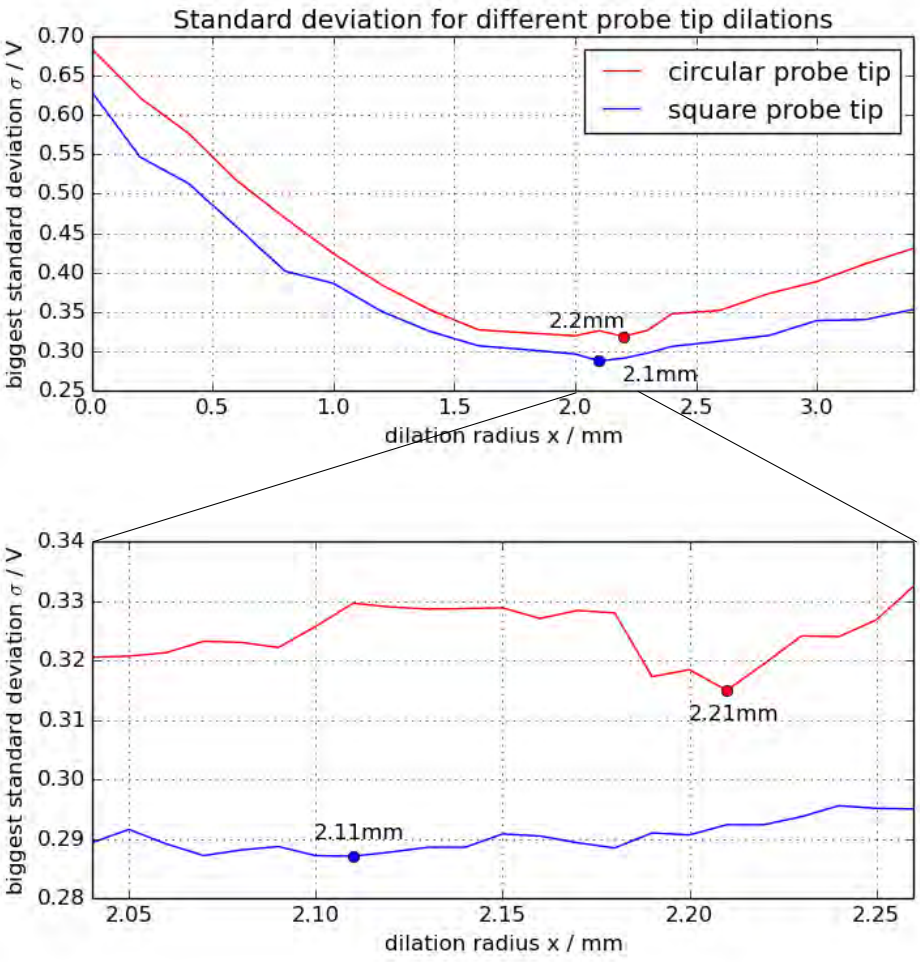

Figure 3.11: This graphs show the standard deviation among normalized loading processes, depending on the dilation radius that was used to compute the compression area. At the first search we tested in steps of $0.2mm$ from $x = 0.0mm$ to $x = 3.4mm$ (top graph). Here, the lowest found standard deviation are at $x = 2.2mm$ and $2.1mm$. In a second, refined search with smaller step sizes of $0.01mm$ (bottom graph), we find that the smallest standard deviation for the circular probe tip is achieved with $x = 2.21mm$ and for the square probe tip with $x = 2.11mm$.

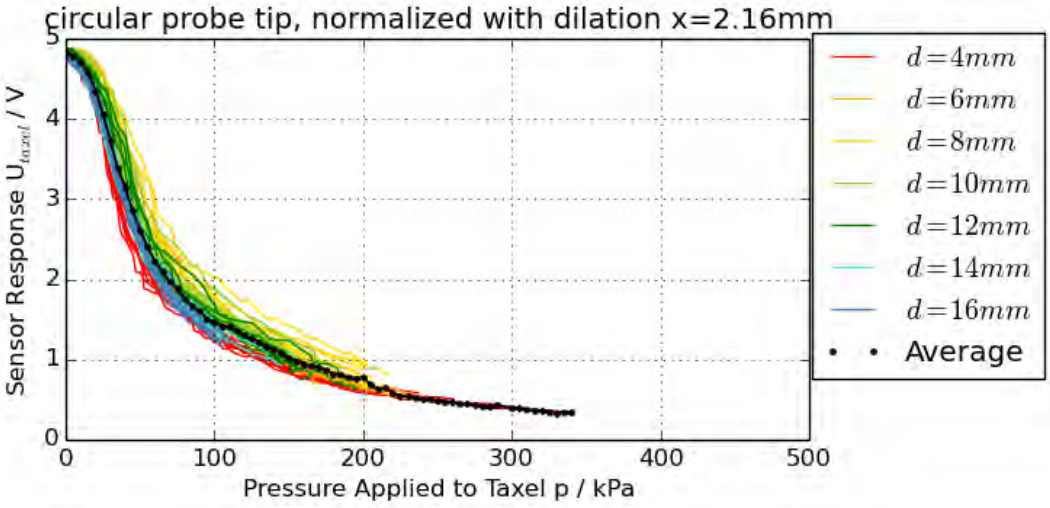

Figure 3.12: The graph shows the sensor response to a loading processes with a circular probe tip. The applied force is normalized to a pressure value using the compression area of the round probe tips. As an estimation of the characeristic line, the average of all sensor resposes over discretized intervals of 5kPa is included in black.

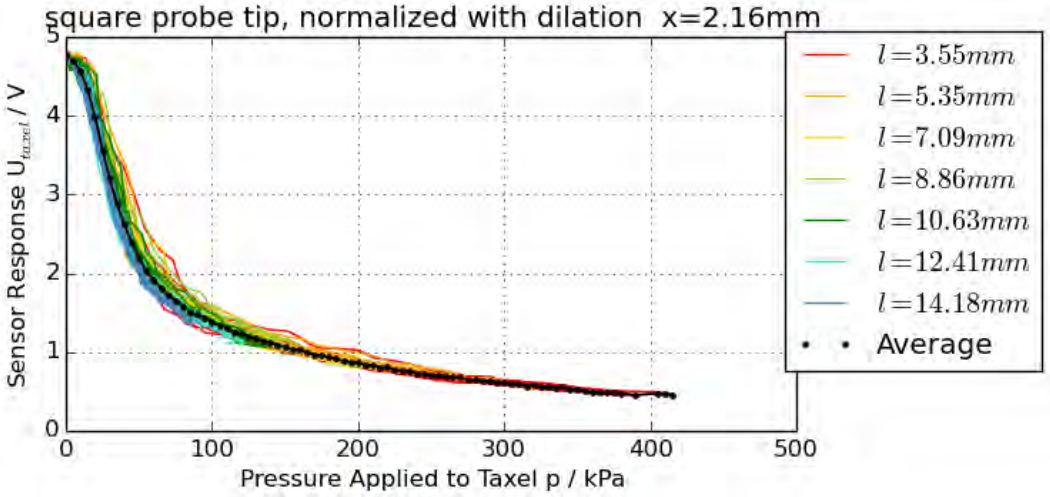

Figure 3.13: The graph shows the sensor response to a loading processes with a square probe tip. The applied force is normalized to a pressure value using the compression area of the square probe tips. As an estimation of the characeristic line, the average of all sensor resposes over discretized intervals of 5kPa is included in black.

dilation radius of $x = 2.16mm$, the average of the two values $x_{circle} = 2.21mm$ and $x_{square} = 2.11mm$.
In Figs. 3.12 and 3.13, this universal dilation radius is applied to normalize the force data from the circular and square probe tips, respectively. All loading processes, independently from their contact area, converge to a line that gives us the relationship between contact pressure as sensor input ans sensor response U_{taxel} as sensor output. A characteristic line is estimated in Figs. 3.12 and 3.13 by the average of the sensor response.

The average lines in the two figures reflect the same relationship between sensor input and output. We conclude that the found line describes a repeatable relationship between the pressure p applied to the sensor and the sensor response U_{out}. This line is valid independently from the size and shape of the contact location. It shows a inverse sigmodial shape that was already described by [18]. For higher contact pressures, approximately beyond 200kPa, the sensor response becomes flatter which makes it harder to distinguish between larges changes in pressure. We can say that the sensor becomes less sensitive for high pressures. The slope of the characteristic line is the steepest between 0 and 80kPa, the sensor is most sensitive to changes in pressure in this range. In the following Sec. 3.2.2 we take a closer look at how this measuring range can be modified.

3.2.2 Sensitivity and Measuring Range

When building up the reading setup as explained in Sec. 3.1.2, we connected each taxel in series with a pull-up resistor to read its sensor output. Based on the voltage divider equation 3.2, the change of resistance of the taxel is always measured in relation to the pull-up resistor. To find the characteristic line of the sensor, we used a constant pull-up resistor of $R_{pullup} = 4.7k\Omega$. In the previous section we learned about the characteristic line of the sensor, but since a different pull-up resistor changes the ratio of the voltage divider we assume that different resistors lead to different characteristic lines.
This is interesting for the applications cases of the sensor when it is applied to soft robotics: When handling light and delicate objects it is important to be able to register small changes in contact pressures. In this case, a high sensibility is crucial for the sensor. On the other side, when handling a variety objects with a wide range of different weights, the sensor needs a large measurement range to detect the range of contact pressures it might experience.
If we find out how the pull-up resistor R_{pullup} changes the characteristic line, the

pull-up resistance could be used as additional variable to customize the sensors sensitivity and measuring range.

We determine the characteristic line for a range of different resistors by exchanging the the pull-up resistor in the experimental setup to various different resistors. For each resistor we record the loading processes on the sensor with the same method as previously, while the probe tip remains at a constant size. With the probe tip size we compute the compression area on the sensor and normalize the applied forces to contact pressures. This way we can approximate the characteristic curve for each pull-up resistor. This will give us insight on how the pull-up resistor affects the sensor response.

In the experimental setup, twelve different pull-up resistors
$R_{pull-up} \in [0.1, 0.33, 0.47, 1, 3.3, 4.7, 10, 33, 47, 100, 330, 470]k\Omega$ are explored. These resistors replace the pull-up resistor in the voltage divider of the sensor reading circuit we used previously, see Fig. 3.4. The setup from the previous section remains unchanged: The F/T sensor is attached to a vertical rail and measures the force it applies to the surface below , see Fig. 3.5. The probe tip that is placed under the F/T sensor is a square shape of 3mm×3mm , which corresponds to the size of a small taxel at the finger tip of the sensor array, and remains unchanged for every loading process. For each of the twelve pull-up resistor 10 of these loading processes are recorded.

All recorded data points are pictured in Fig. 3.14. All loading processes have the inverse sigmodial shape in common. The higher the pull-up resistor, the steeper is the slope of the sensor response, an the faster the sensor output converges towards $U_{taxel} = 0V$.
The slope corresponds to the sensitivity of the sensor and its ability to response to small changes in contact pressure. The higher the pull-up resistor, the higher the slope and the higher the sensitivity of the sensor. As the sensor output converges close to $U_{taxel} = 0V$, the slope flattens out and big changes of pressure evoke only small changes in the sensor output. At this point, the compression of the sensor made the resistance of the sensor drop to an insignificant amount compared to the pull-up resistor. The lower the pull-up resistor, the more compression needs to be applied to the piezoresistive fabric reach this critical resistance. This means that the measuring range of the sensor increases with the pull-up resistor.
Sensitivity and measuring range are counteracting each other as gaining one means

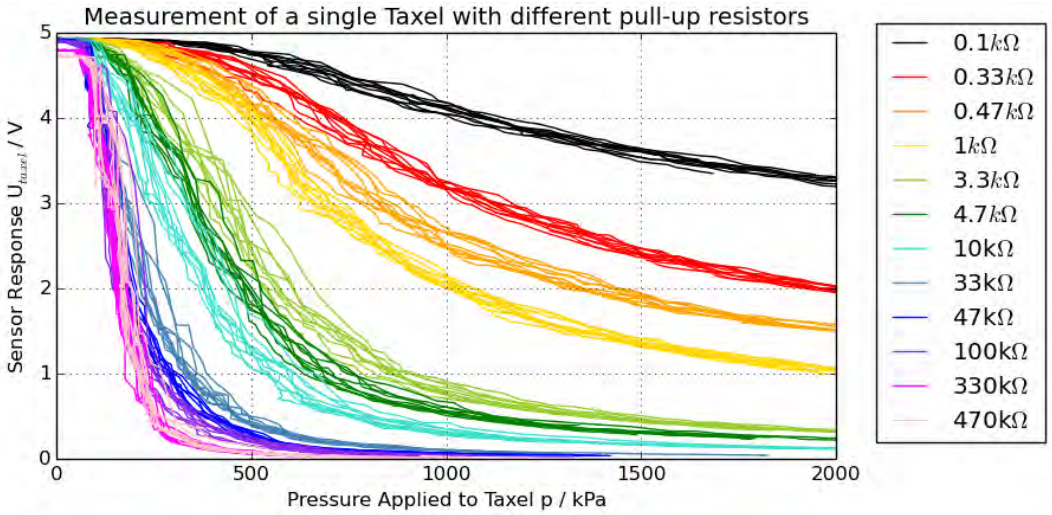

Figure 3.14: The graph shows the sensor response to contact pressure with different pull-up resistors. All loading processes were produced by a square 3mm×3mm probe tip. The loading processes recorded with the same pull-up resistor R_{pullup} are depicted in the same color.

the decrease of the other.

In conclusion, the pull-up resistor R_{pullup} in the voltage-divider determines the sensitivity and the measurement range of the sensor. It is therefore a useful parameter to adapt the sensor properties according to its needs. Before each usage of the sensor array we have to consider which is more important to the application, a wide measurement range or a high sensor sensibility, and adjust the pull-up resistor accordingly.

4 Tactile Gripper

4.1 The RBO Hand 2

The RBO Hand 2 is the latest model of several soft hand developed at the Robotics and Biology Laboratory at Technische Universität Berlin. Made from only soft materials, the compliance of the RBO Hand allows to experiment on morphological computation. The compliance of the hand does not allow exact modelling, planning or control. Instead, low levels of control are taken over by the soft body of the hand. For example, the morphology of the gripper performs the small corrections and re-adjustments that are necessary to perform a stable grasp on a wide range of objects. The tactile sensor array proposed in this work is partly motivated by the goal to add tactile sensing to the RBO Hand 2.

The RBO Hand 2 is made from several soft PneuFlex actuators [24]. They are attatched to a 3D-printed scaffold and roughly follows the shape of a right hand. Each PneuFlex actuator is made from silicone rubber and has an air compartment on the inside which can be inflated with compressed air. During the inflation, the actuator is restricted by a silk sheet reinforcement that is embedded in the silicone and a thread that wraps around the entire actuator like a helix. These restrictions provide the direction in which the actuator expands and define its morphology. The silk sheet reinforcement is placed on the surfaces that face the palm of the hand and prevents the silicon from expanding. As a result, the actuators curl towards the palm of the hand upon inflation and clench to a fist. To open the hand, the air pressure is released from the actuators, and due to the elastic properties of the silicon the actuators return to their previous position.

The RBO Hand 2 used in in the scope of this work has a special version of the PneuFlex actuator for the index, middle, ring and little finger. Instead of one air compartments, this version has two air compartments which can be inflated independently through two air tubes located at the base of the finger. The bottom compartment bends the finger at the finger base, while the top air compartment activates a deflection of the top half of the finger. Together with the two actuators of the palm and one compartment in the thumb, this RBO Hand 2 has a total of 11 individual air compartments. The position of all compartments is visualized in Figure 4.1.

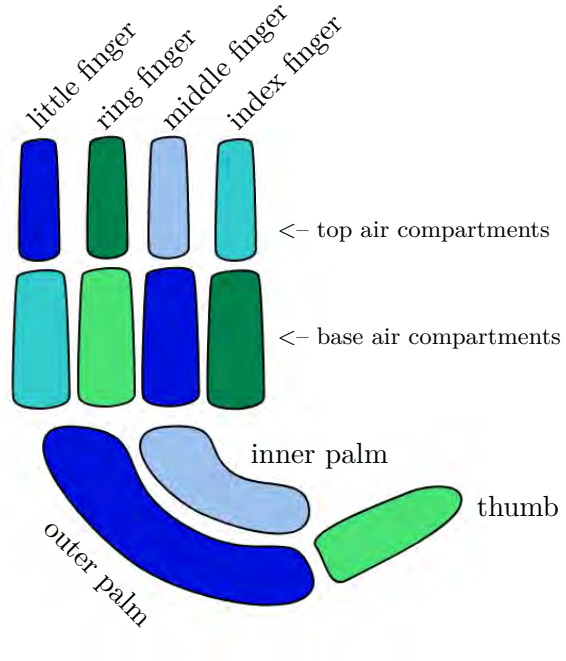

Figure 4.1: The RBO Hand 2 has seven PneuFlex actuators, five fingers that connected to the two-piece palm of the hand. In this figure, the palm of the hand is facing upwards. The index, middle, ring and little finger each contain two independent air compartments, one in the top of the finger and one at the base of the finger. The thumb actuator contains only one compartment. The palm of the hand is made from two actuators, each with one air compartment. In total, this RBO Hand 2 has 11 independent air compartments.

The the soft hand is actuated by air pressure in the air compartments. The necessary airflow is provided by an external air compressor and controlled by a custom control unit, the PneumaticBox. Six valves that are integrated in the PneumaticBox allow the actuation of six independent air compartments. An embedded computer contains the software stack that allows realtime control of the mass flow in the air valves. An additional diver board in the Pneumatic Box contains the drivers for the valves an pressure sensors.
With the realtime control handler, which is part of the software stack, we can record and replay actuation states. To record a state, each air compartment is inflated to the desired degree and the air mass used for each compartment is then saved as that state. To replay the same state, the controller reproduces the mass flow. After recording multiple states, they can be replayed as a sequence to execute complex movements.

The pressure sensors of the diver board measure the air pressure inside each air compartment. This provides us with a sensory feedback. Since the air pressure sensors are located on the driver board of the PneumaticBox, they measure contacts in an indirect way; If an actuator experiences external contact pressure, it can be measured as an increase of the internal air pressure.
Since each PneumaticBox only has six valves, two PneumaticBoxes are required for the operation of the RBO Hand 2 with 11 independent air compartment. This also allows the recording of all 11 air pressure values from the compartments.

4.2 Integration of the Tactile Sensor Array

In order to use the proposed tactile sensor array with the RBO Hand 2, we need to attach the sensor to the soft hand. The shape of the tactile sensor follows the outline of the PneuFlex actuators that are used for the index, middle, ring, and middle finger. These are the four fingers we sensorize. The two palm actuators and the thumb actuator are each of a different shapes and are not fitted with tactile sensors in the scope of this work.
In the way we attach the sensor array to the actuator we have to consider two constraints. Firstly, the PneuFlex actuators are made from silicone. Silicone has the property that nothing can stick to it besides silicon or special silicone glue. The second constraint is a lesson we learned during the manufacturing of the sensor array. When we tested different adhesives to combine the layers of the sensor, we

found that liquid glue soaks into the fabric layers of the sensor and change their conductive properties. [7, Ch. 3] proposes multiple strategies to integrate a sensor to a soft actuator. The suggestion include:

1. Embedding the sensor in the top silicon layer during the manufacturing process of the actuator
2. Attaching the tactile sensor to a glove that can be worn by the soft hand
3. Attaching the sensor directly to the actuator surface with an adhesive

Embedding the sensor into the surface of the actuator had the advantage that the sensor itself is protected by a silicon layer. Being exposed to the contact pressures is necessary to measure them, but also puts a strain on the sensor during every interaction. A protective silicon layer around the sensor could increase its durability and lifespan. On the other side, both the PneuFlex actuator and the tactile sensor array are time-expensive to manufacture. If the sensor is embedded into the actuator, they are irreversibly merged and a defect on either of them renders them both useless. We therefore prefer to build the actuators and the tactile sensor array separately and connect them at the end of the manufacturing process. This has the advantages that, in case of a defect on either the actuator or the sensor, the still functioning half can be re-used. If the actuator breaks, the attached sensor can be transferred to a new actuator, or a broken sensor can be removed from a finger and be replaced. An other option is the integration of the sensor to a tactile data glove that is pulled over the soft hand. [25] build such a tactile glove for human hands. Their taxels are etched on a conductive fabric and could therefore be sewn together to form a tactile glove. Sewing our proposed sensor would perforate the flexPCB layer and potentially break the sensor.

This leads to the third sensor integration strategy, attaching the sensor to the surface of the actuator with an adhesive. Since the fabric layers of the sensor are affected by liquid silicon glue we can not apply the adhesive directly on the sensor. Non-liquid adhesices such as double-sided adhesive tape on the other side does not stick on the silicone actuator.
To protect their sensor from its environment, [19] used a water-proof iron-on vinyl fabric to surround their fabric based tactile sensor. The plastic base material of our flexPCB is not heat-resistant, therefore it is not possible to apply any material with a hot iron. Instead, we manufacture a silicon sleeves that covers the whole length of the tactile sensor.

The sleeve is produced separately from the sensor, in the same shape as the tactile

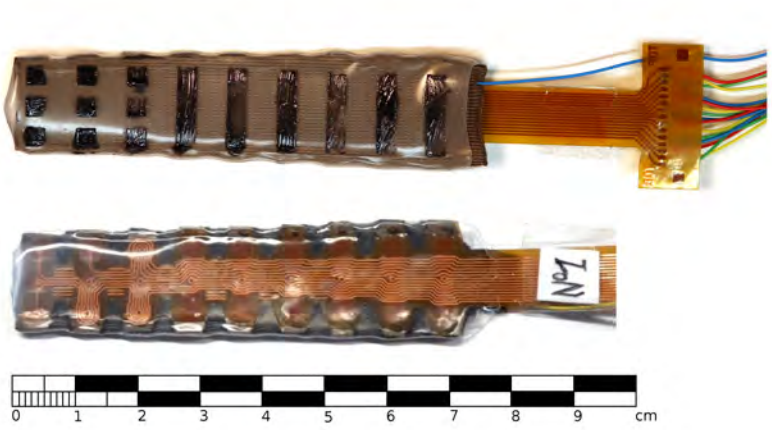

Figure 4.2: A thin silicon sleeve is placed around the sensor array. The sleeve protects the sensor from liquid glue entering the fabric layers of the sensor and allows us to glue the sensor on the PneuFlex actuator. On the sleeve, the location of the taxels are marked with black dyed silicon on the side where the flexPCB is not visible. This acts as a visual guide to where the taxels are located.

sensor array. The outlines of the sensor are cut from a 3mm thick sheet of acrylic glass to crate a casting mold in the shape of the sensor. The corners of the mold are rounded off with sandpaper. Then, the mold is covered with Dragon Skin 10™ silicone by Smooth-On (US-PA) and hung up to cure. When the silicone is dry we apply a second layer of Dragon Skin 10. After the silicon is cured a second time it can be peeled of the mold and placed on the sensor like a sock. With this sleeve, the sensor layers are airtight protected from liquid adhesive soaking in the material. Figure 4.2 shows the final sleeve as it's placed on the tactile sensor array.

With this sleeve placed on the sensor, we can use the liquid silicon glue to attach the sensor to the actuator surface. The are two orientations in which we can attach the sensor: Either the FlexPCB is facing the actuator or it is facing away. Once the sensor is attached to the actuator, the actuator itself and its inflation can affect the sensor output. The goal is to find the sensor orientation in which the influence of the actuator on the sensor output is minimized.

We take two PneFlex actuators and two tactile sensor arrays which are covered by a silicone sleeve. The sensors are attached to the actuators, one with the flexPCB facing the actuator and one with the flexPCB facing away. We define six states of inflation of the actuator. While we traverse the six states with each actuator, we

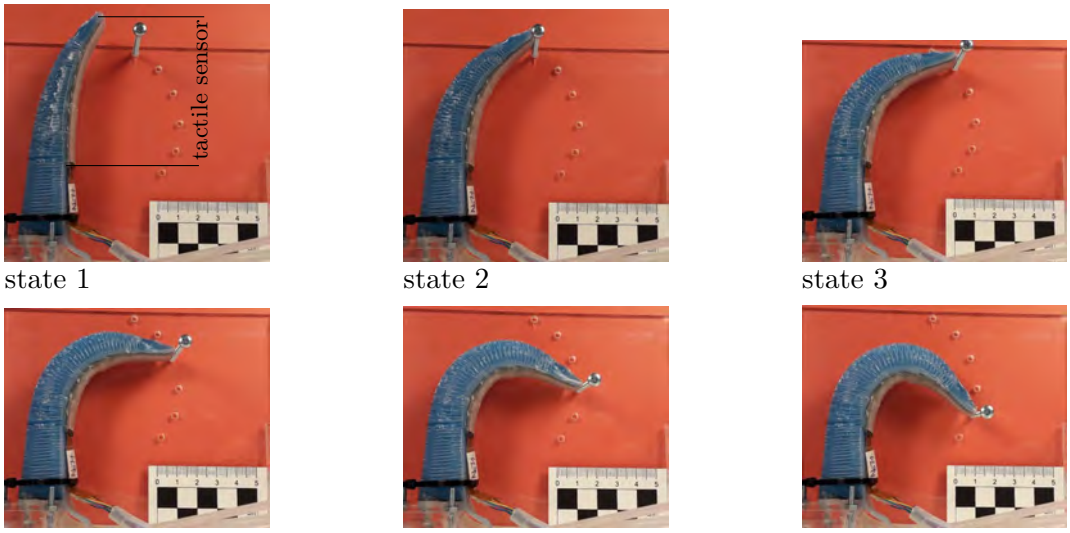

Figure 4.3: These pictures show a two compartment PneuFlex actuator with a tactile sensor array attached to it. We define six actuation states based on the arch described of the finger tip upon inflation of the top air compartment. In the first state, the actuator is not inflated. The following states 2-6 are marked with holes on the acrylic glass in the background and show a gradual inflation. On the pictures, a sixth hole for a seventh state is visible. Unfortunately, the maximum inflation of the two used actuators were located on different locations on the arch, and one of the tested actuators was unable to reach the seventh state.It was therefore dropped from this experiment.

observe the sensory output attached sensor array. For every taxel of the sensors we register how much of the measurement range is triggered by the actuation. Since the sensor cover approximately the top 70% of the actuator, we focus on the bending that occurs in the upper part of the actuator which is caused by the inflation of the upper air compartment. The bottom compartment causes the actuator to bend at a point close to the finger base that is located below the tactile sensor.

We define the six actuation states where the tactile sensor experiences different degrees of bending. We mounted the actuator to the ground surface, behind it we fixed a acrylic glass plate on which we marked the arch the fingertip of the actuator draws when the top compartment is inflated. On this arch we drill evenly spaced holes that mark each state. These six states are pictured in Figure 4.3. In the first state, the actuator is not inflated at all. To reach the following states, we screw a screw in the hole that corresponds to that state and inflate the top compartment until the finger tip reaches the screw. This way we ensure that both actuators with the sensor orientations we want to test have the same deflection when we record the sensor response of the tactile array. Over each state, the top compartment of the

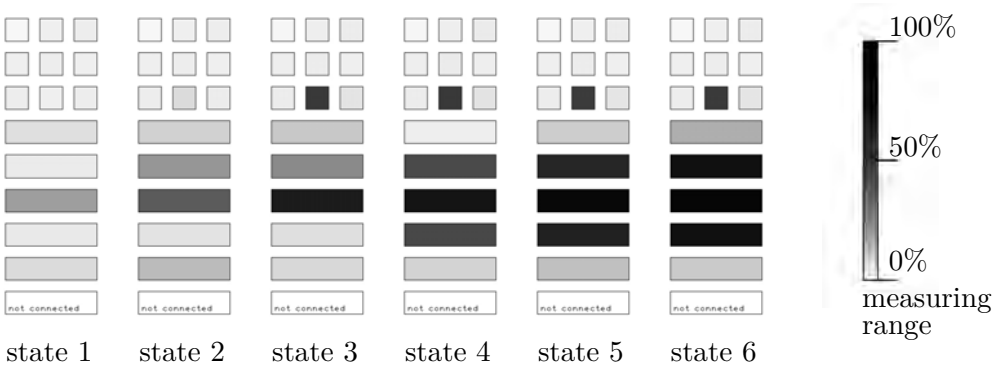

Figure 4.4: This heat maps show the measured contact pressure for 6 different actuation states if the sensor is attached to the actuator with the flexPCB facing away from the actuator. The heat map of the measured contact pressures is displayed as percentage of the measuring range for each taxel. White indicates no contact pressure, while black indicates that the full measuring range of the taxel is exhausted.

actuator is gradually inflated, until it reaches its maximal inflation state 6. As we reach each state, we record the sensor response of all 14 taxels of the tactile sensor array. This is repeated once with each of the two sensor orientations.

The sensor response for each taxel can range between $U_{taxel} = 5V$ if no contact pressure occurs and close to $U_{taxel} = 0$ if the contact pressure of the taxel exceeds measurement range. The sensor response of each taxel is visualized in a heat map. The colour of each taxel displays in a percentage how much of the measurement range is exhausted by the inflation. 0% means that the output of the taxel is not affected by the inflation, at 100% the taxel output droped from 5V to 0V due to the inflation. The sensor response of the sensor attached with the flexPCB facing away from the the actuator is visualized in Fig. 4.4. In the not inflated state (state 1) the sensor already displays a contact pressure at the center taxels. This increases with increasing inflation of the top air compartment. At state 3, one central taxel already displays 100% of the contact pressure it can measure. According to the pictures in Fig. 4.3 this corresponds to the location where the inflation of the actuator bends the tactile sensor most. The tactile sensor experiences the most deformation here. In comparison, the tactile sensor response of a sensor that is attached with the the sensor facing the actuator is displayed in Figure 4.5. In the first two actuation states it shows no contact pressure at all, after state 3 the pressure begins to increase on the central taxels.

Overall, the contact pressure inflicted by the actuator inflation is significantly smaller

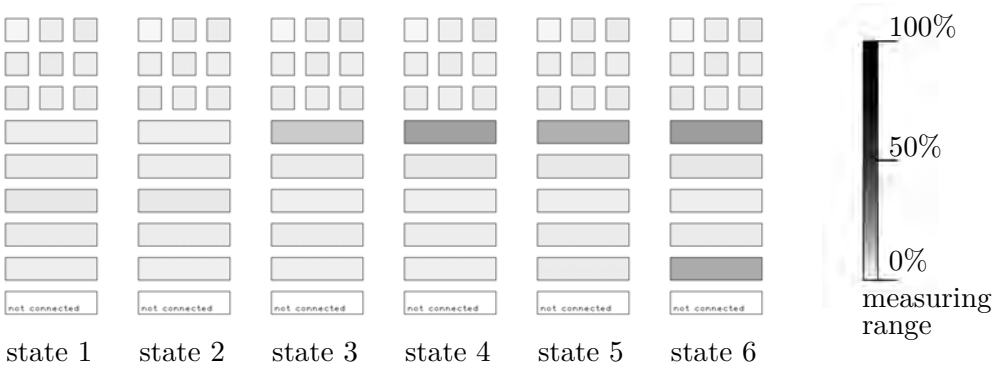

Figure 4.5: This heat maps show the measured contact pressure for 6 different actuation states if the sensor is attached to the actuator with the flexPCB facing the actuator. The heat map of the measured contact pressures is displayed as percentage of the measuring range for each taxel. White indicates no contact pressure, while black indicates that the full measuring range of the taxel is exhausted.

if the flexPCB is facing the actuator. The different performances for the two sensor orientations can be explained with the properties of the flexPCB. When the actuator inflates, it expands and presses against the sensor, resulting in the sensor to measure a contact force that originates in the actuator and not in a contact with the environment. Among all layers of the tactile sensor array, the flexPCB is the stiffest. It can comply with the movement of the actuator, but small local pressures are distributed to a larger surface before they are passed on to the underlying fabric layers. When facing the actuator the flexPCB can, to a limited degree, shield the piezoresistive layer from the pressure of the actuator inflation.
The pressure that is measured by the taxels in the middle of the sensor array can not be avoided, only minimized by the orientation of the sensor. As soon as the sensor is bend over a certain degree, the fabric on the sensor forms small crinkles on its surface. In these crinkles, the fabric experiences compression and therefore changes its resistive properties. With the pull-up resistor we have the option to adjust the sensitivity of the sensor array to minimize this effect. But this would cost us the option to use the sensor with a high sensitivity and is therefore not feasible.

Based on the results we conclude that the actuator is better placed on the actuator with the flexPCB facing the actuator. Applied to out soft hand, we now attach four tactile sensor arrays to the RBO Hand 2. Figure 4.6 shows the final RBO Hand 2 with four tactile sensors at the index, middle, ring, and little finger.

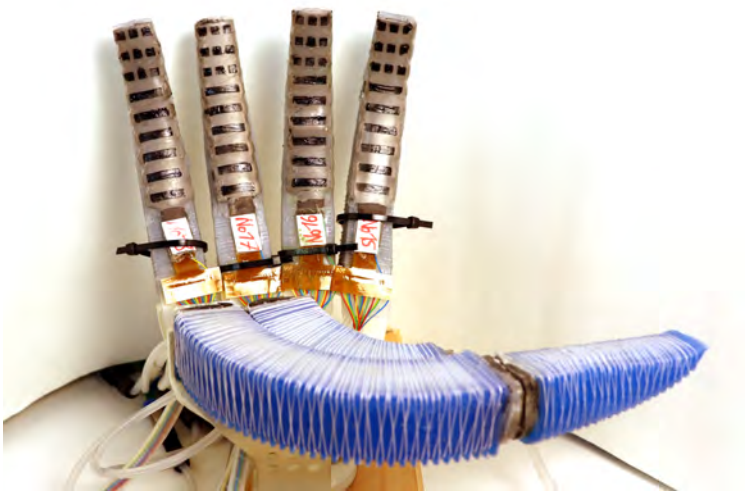

Figure 4.6: A tactile sensor array is attatched to the index, middle, ring and little finger of this RBO Hand 2. The flexPCB of each sensor is facing the actuator.

4.3 Evaluation of the Sensor Integration

The compliance of the soft actuators is a great advantage of the soft hand. Therefore it was an important objective of the sensor design to make the tactile sensor array not restrictive to the movement of the actuators. With this objective in mind we chose the materials to manufacture the tactile sensor, namely the flexPCB, the piezoresistive and conductive fabric, and the adhesive tape to connect these materials. After the integration of the tactile sensor to the PneuFlex actuators, we reassess if and to which extend the compliance of the actuators has changed due to the addition of the sensor.

Due to its compliant properties, the PneuFlex actuator can yield in different directions under an external force. We test this compliance in three different directions: To the front (flexion), to the back (extention) and sideways (abduction), see Fig. 4.7. To quantify the compliance of the actuator, we deform an actuator with attached tactile sensor and an actuator without tactile sensor with defined forces. For each applied force we record the displacement compared to the relaxed position of the actuator. The measured displacement of the finger tip serves as indicator of the compliance of the actuators. By comparing the compliance of the two actuators we can infer the effect of the tactile sensor array on their compliance.

In this experimental setup, it is necessary to apply a pull to the finger tip of a

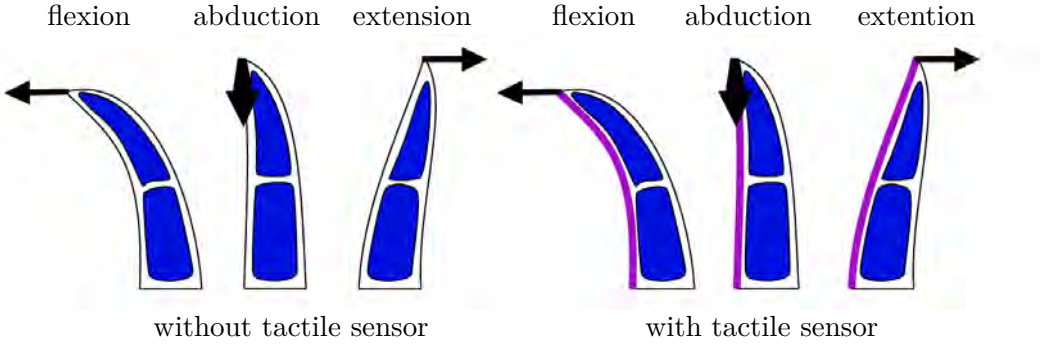

Figure 4.7: To explore if and how the tactile sensor array changes the compliance of the PneuFlex actuator, we bend it in three directions: To the front, the back, and sideways. This figure shows cross-sections of the sensorized PneuFlex actuator. On the left side, its two compartments in blue can be seen. On the right side the attached tactile sensor array is added in purple. On the left and the right side, the three black arrows show the directions in which we test the compliance of the actuator.

PneuFlex actuator. This pull is applied with a force gauge. A iron spring inside the gauge is stretched under the pulling and displays the force on a scale. To hook the force gauge to the tip of each actuator we sewed a plastic ring to the finger tip of each actuator. Because the stitches perforate the flexPCB at the finger tip and destroy its functionality, we use the actuator from the previous section where the flexPCB is facing away from the actuator.

Each PneuFlex actuator is fixed by its base on an horizontal table top, with a plain surface in the background. On this background we mark the position of the finger tip in a neutral state when no pull is applied. With a force gauge, which is hooked to the ring, we apply a series of defined pull forces on the tip of the actuator. In each of the three directions, we pull the actuator tip with $F \in [1, 2, 3, 4]N$. For each force, the position of the tip of the actuator is marked on the background surface. Fig. 4.8 shows the deformations we observed during the experiment.

For each of the three directions, the displacement of the finger tip is recorded three times. The results for the flexion/extention are shown together in Fig. 4.9, During extention, the actuator with a tactile sensor shows approx. 25% less displacement compared to the unsensorized actuator. The flexPCB of the sensor is flexible, but not elastic, and can not stretch when the actuator is extended. It therefore adds a layer of reinforcement to the palmar side of the actuator. During flexion on the other side the sensorized actuator shows a higher displacement compared to the unsensorized actuator.

During abduction, the results in Fig. 4.10 show that the tactile sensor has no signif-

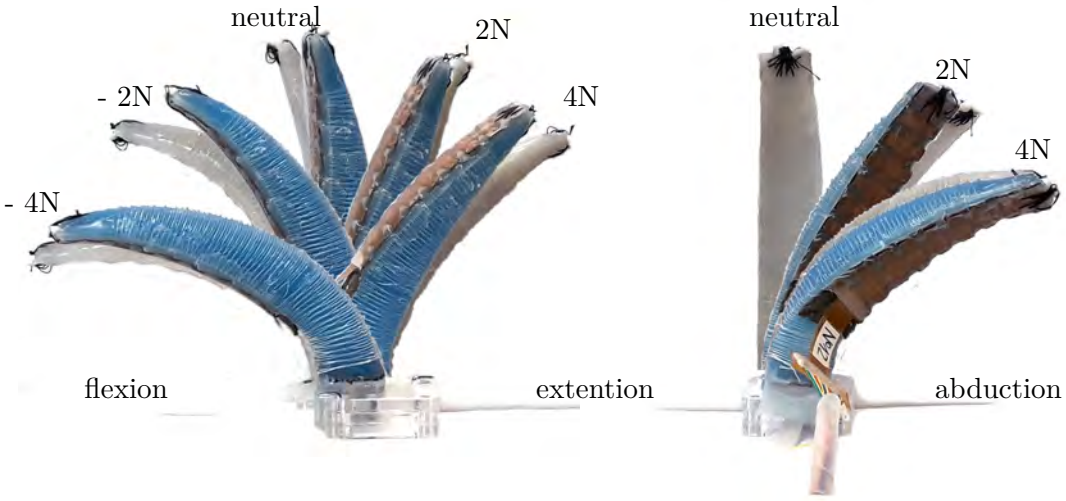

Figure 4.8: We determine the influence of the tactile sensor array on the compliance of the PneuFlex actuator. On an actuator with a tactile sensor attached (blue) and an actuator without tactile sensor (grey) we apply pulling forces to their finger tips with a force gauge and observe their deformation. In this images, only the deformation for 2N and 4N are displayed.

icant impact on the compliance of the actuator. As apparent in Fig. 4.8 (right side), both actuators avoid to bend sideways under a lateral force. Instead they perform a twist motion around their own axis to face their palmar side in the direction of deformation, and subsequently perform a flexion. This behaviour is predefined by the morphology of the PneuFlex actuator. During manufacturing, the palmar side is reinforced with a non-elastic fabric that is embedded in the silicone. This fabric enables the flexion of the actuator in the first place but also prevents a true sideways bending.

We have to assume that every addition to the actuator will change its morphology and therefore its compliant behavior. The proposed sensor and the integration strategy we chose impacts the extension of the PneuFlex actuator by reducing its compliance by approx. 25%. The extension of the actuator occurs usually when the actuator is forcefully bend backwards while it's not actuated. The primary direction of actuation remains the flexion. In this context, this reduced compliance of the extension is not significant for the functionality of the actuator.

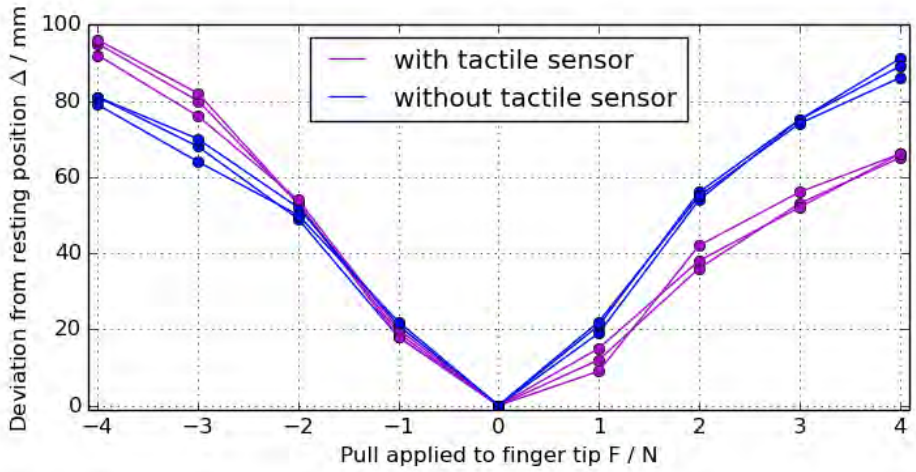

Figure 4.9: The actuator is displaces from its neutral position (0N) by pulling forces. During flexion (in negative direction), noth actuators show the same deformation for small forces. For the higher forces, the actuator with an sensor attached shows a slightly higher displacement. During extention (in positive direction), the actuator with an sensor attached shows consistently a smaller displacement.

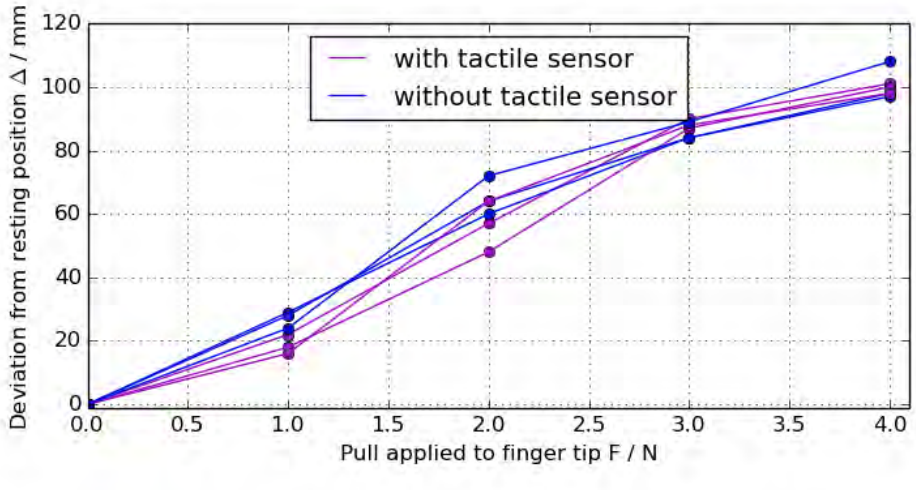

Figure 4.10: caption

5 In-Hand Object Recognition

When the pneumatic gripper grasps an object, it produces a contact pattern on the inside of the hand, with different contact pressures and locations depending on the shape of the object. With the high spatial resolution of the sensor array, we can distinguish between different contact locations on the surface of each finger, an the continuous measurement indicates the different contact pressures at each individual taxel. Together they form a pattern a classifier can learn do distinguish.
To explore the ability of the tactile sensor to recognize different objects, we choose a set of objects with diverse properties regarding shape and softness. While we grasp each of these objects with the sensorized soft hand, we record the sensor response of the tactile sensors. At the same time, we record the sensor response of the air pressure sensors that are located in the PneumaticBox. They measure the air pressure inside the air compartments of the actuators.
The data from both sensor types, the tactile sensors as well as the air pressure sensors, is used to classify the grasped objects. This gives us the opportunity to compare the classification accuracy of the two sensor types. Since only the four large fingers of the the soft hand are equipped with tactile sensor, we just use the air pressure data of these four fingers (see Fig. 4.1 for an overview of all air compartments of the RBO Hand 2).
To compare the classification of both sensor types, we search for the best classifier for both the tactile and the air pressure sensors. With such optimized classifiers, we take a closer look at the classification results. We are particularly interested in how well the classifiers can distinguish between the properties of the different objects. We also take a closer look at how the high spatial resolution of the tactile sensor contributes to the object recognition.

5.1 Experimental Setup and Data Acquisition

For the object recognition, we composed an object set of nine different everyday objects. Based on their properties, we divide the set into three object groups:
The first group, *"Objects in Packaging"*, includes a plastic bag of cat treats, a plastic bag of chopsticks and a pair of safety glasses in its original plastic wrapping (see figure 5.1). The three objects can move freely inside their packaging. The cat treat, consisting of small bit, can thereby move in every direction, while the chopsticks

Figure 5.1: Objects Group One: Objects in Packaging. It contains a plastic bag of cat treats, a plastic bag of chopsticks and a pair of safety glasses.

Figure 5.2: Objects Group Two: Plastic Bottles. It contains a bottle of whiteboard cleaner, a plastic gum container, and a bottle of school glue.

Figure 5.3: Objects Group Three: Balls. It includes a tennis ball, a soft stress ball and a toy gel ball.

can only turn parallel to each other The safety glasses are, different that the other two objects of the group, made from only one piece inside the packaging but has a irregular shape.
"Plastic Bottles" form the second object group. It contains a bottle of whiteboard cleaner, a plastic gum container, and a bottle of school glue (see figure 5.2). All three objects in this group have a smooth surface and a rigid shape in common. The gum container and the whiteboard cleaner both have a cylindrical shape, with the cum container having a slightly larger diameter. The school glue on the other side has a oval footprint.
As third group, we picked different *"Balls"*. It includes a tennis ball, a soft stress ball and a toy gel ball (see figure 5.3). The three balls have approximately the same diameter, but their softness are different. The tennis ball is the most rigid, barely deformable by hand. The soft ball can be compressed with a slight effort, while the gel ball is the softest of the three. It yields and deform even under small pressures.

During the data acquisition process, the tactile gripper is fixed on the table top by its wrist. The palm of the hand is facing upwards. The air flow to the compartments of the hand are controlled by the PneumaticBox, while the air pressure sensors in the PneumaticBox measure the air pressure inside the air compartments. Chapter 4.1 contains more detailed information about the control of the RBO Hand 2. The four tactile sensor arrays of the hand are connected to solderless plug-in beadboards. On the breadboards are a total of 56 voltage dividers, one for every taxel on the hand. The output of the voltage dividers are read by four Labjack U6 (A/D), each one with 14 analog inputs that are sufficient for one tactile sensor array. The complete setup of the tactile gripper is visualized in figure 5.4.

To acquire the data of the two sensor types during a grasp, we first record a sequence of actuation states. During the sequence the hand closes to a fist, holds that positions for 3 seconds to allow all sensor values to stabilize. Then, the sensor outputs of the tactile sensor and the air pressure sensor are recorded, before finally all air pressure is released again to open the fist. To replay the sequence, the PneumaticBox uses the same air mass flow for the inflation of each actuator, which assures the same grasp for every repetition. This sequence can be replayed as often as needed, and we use the same grasp for every item of the object set.
Since the hand is mounted to the table top with the palm facing up, we can now place the objects from our object set in the palm before the hand closes. Each of the 9 objects from the set is places in the hand 30 times. Between each grasp, the

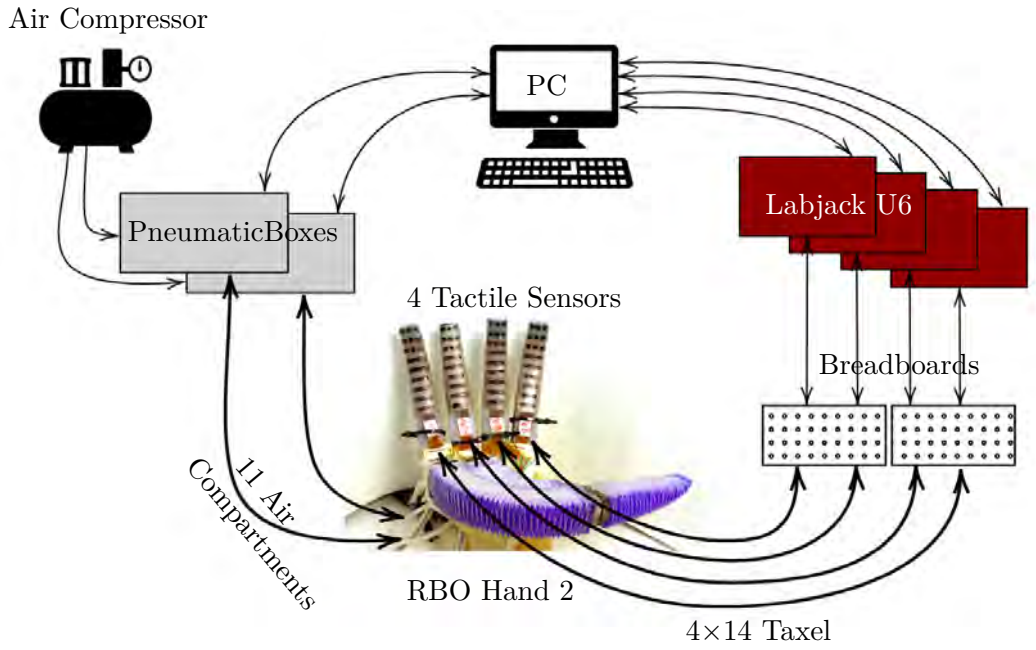

Figure 5.4: In the experimental setup for the in-hand object recognition, the gripper is fixed to the tabletop, with the palm facing up. The air mass flow to each of the 11 air compartments is controlled by two PneumaticBoxes. They also contain pressure sensors for each air compartment. The four tactile sensor that are equipped to the RBO Hand 2 are connected to two breadboards with 28 voltage dividers each. From there four Labjack U6, one for each tactie sensor array, reads the tactile sensor output.

object is removed from the hand, rotated by a random amount and placed back in the palm of the hand. With this method we make sure the objects are grasped from different angles.
In the end we have two data sets of grasps, one for the tactile sensor and one for the air pressure sensor. Each data set contains 270 data points (9 object labels that occur 30 times each). A data point of the tactile sensor has 56 dimension, resulting from 4 tactile sensors with 14 taxels each. A data point of the air pressure sensor has 11 dimension that contains the 11 air pressure values from all air compartments. Three of these values are from the two palm actuators and the thumb. Since these actuators are not equipped with tactile sensors, we also refrain from using their air pressure values. As a result, in the following we will use only the 8 dimensions that contain the air pressure data of the four sensorized fingers.

5.2 Classification Results

To get the best possible prediction for each sensor type, we compare different machine learning techniques for classification: The decision tree classifier, the k-neighbour classifier and support vector machine (SVM). The k-neighbour classifier can use either uniform or weighted distance wights, therefore we explore both. The SVM we test with three different kernels: Radial basis function (RBF) kernel, polinomial kernel and linear kernel.
Each classifier is scored by its accuracy, which is computed by a leave-one-out cross-validation. From all 270 data points we remove one point as test point, and train the model with the remaining 269. With the trained model, we predict the label of the test point. This is performed 270 times, each time a different data point is removed as test point, until we have a predicted label for each data point. The accuracy is then computed by the fraction of correctly labelled data points among all data points. It can range from 0 to 1, which corresponds to $0 - 100\%$ classification accuracy.

The SVM classifier depends on their own hyperparameter, which strongly impact the performance of the classifier and can not be trained. The RBF kernel and polynomial kernel depend on the parameters C and gamma γ, the linear kernel depends only on the parameter C. The parameter C controls the trade-off between clear boundaries in the decision making on one side and the correct classification of each training point on the other. The smaller C, the lower the training accuracy, but we enable a larger the decision margin. The parameter gamma γ on the other side

Table 5.1: The classification results for every tested classifier, each of them trained once on the tactilse sensor data and once on the air pressure data. For each kernel of the SVM classifier we performed a grid search on their hyperparameter to get the optimal classification result.

Classifier	**Tactile Sensor**	**Air Pressure Sensor**
Decision Tree Classifier	73.33%	66.30%
K-Neighbors Classifier uniform weight	77.78%	55.19%
K-Neighbors Classifier distance weight	79.63%	55.19%
SVM with Polynomial Kernel	87.40% with parameters $C = 20$, $\gamma = 0.001$	71.48% with parameters $C = 0.05$, $\gamma = 0.001$
SVM with RBF Kernel	89.25% with parameters $C = 10$, $\gamma = 0.009$ or $C = 11 - 14$, $\gamma = 0.007$	72.96% with parameters $C = 1000$, $\gamma = 0.0001$
SVM with Linear Kernel	88.15% with parameter $C = 0.1$	69.25% with parameter $C = 1$

determines how far the influence of one single data point extends. For a high gamma value, only data points close to the decision boundary have an influence on its shape. This gives few data points a lot of impact. The lower the gamma value, more data points that are further away from the decision boundary are considered when the decision boundary is drawn.
To be able to compare the SVM classifiers effectively to the others classifiers, we optimize these two hyperparameters for each SVM classifier in a grid search. Again, we use the accuracy to score each combination of parameters in the grid. If necessary, the search grid is refined for the best parameter range.

The prediction accuracy of each optimized classifiers is listed in table 5.1. For both sensor types, the SVM classifier with a RBF kernel achieves the highest classification rate. In Figs. 5.5 and 5.6 we visualized the grid searches to find the best parameters for the SVM classifier. When trained on the tactile sensor data, the classifier achieves a total prediction accuracy of 89.26%. Compared to that, the classifier only reaches an prediction score of 72.96% when trained on the air pressure data.

With the optimal classifier found, we now take a closer look at the classification rate of each object of the object set. The results of the classification based on the tactile sensor array is shown in Fig. 5.7. The three objects in packaging, located in the top left corner, show the lowest classification accuracy of 73% - 89%. The plastic bottles reach the highest recognition rate, with the gum container and

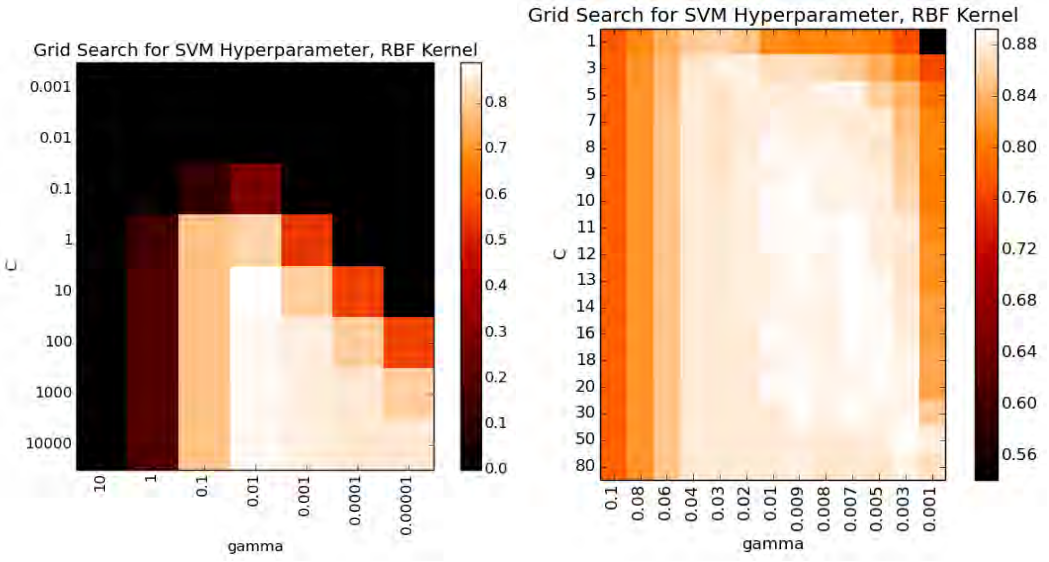

Figure 5.5: Based on the tactile sensor data, we optimize the hyperparameters of the SVM with RBF kernel with a grid search. Each parameter set is scored by a take-one-out cross-validation. In the first grid search we explore a wide range of values (left). Based on these first results we refine our search in the second grid around the parameter set $[C, \gamma] = [10, 0.01]$. In the second search the highest score of 89.26% is achieved with the parameter sets $[C, \gamma] \in [[10, 0.009], [11, 0.007], [12, 0.007], [13, 0.007], [14, 0.007]]$

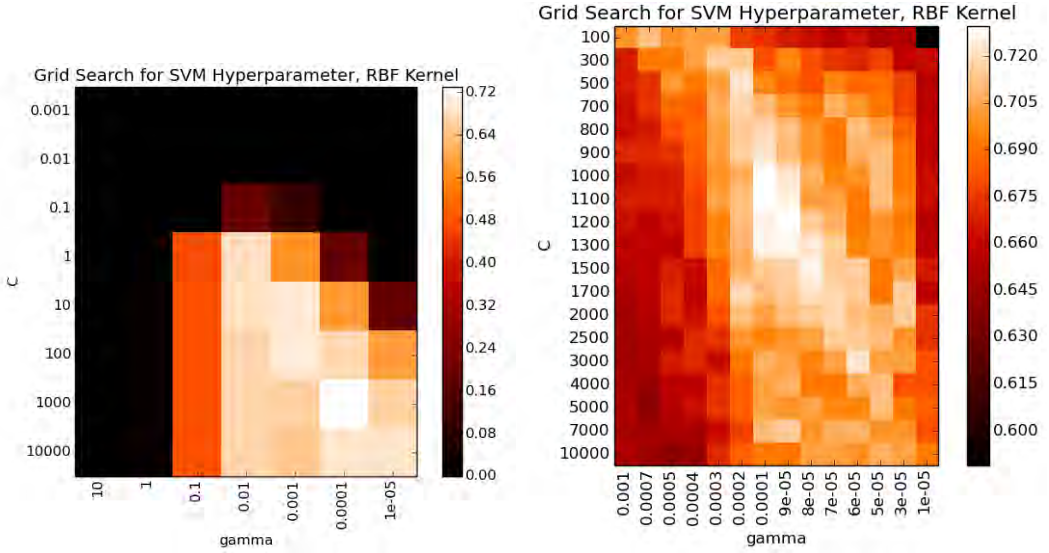

Figure 5.6: Based on the air pressure sensor data, we optimize the hyperparameters of the SVM with RBF kernel with a grid search. Each parameter set is scored by a take-one-out cross-validation. In the first grid search we explore a wide range of values (left). Based on these first results we refine our search in the second grid around the parameter set $[C, \gamma] = [1000, 0.0001]$. In the second search the highest score of 72.96% is achieved with the parameter sets $[C, \gamma] \in [[1000, 0.0001], [1100, 0.0001], [1200, 0.00009]]$

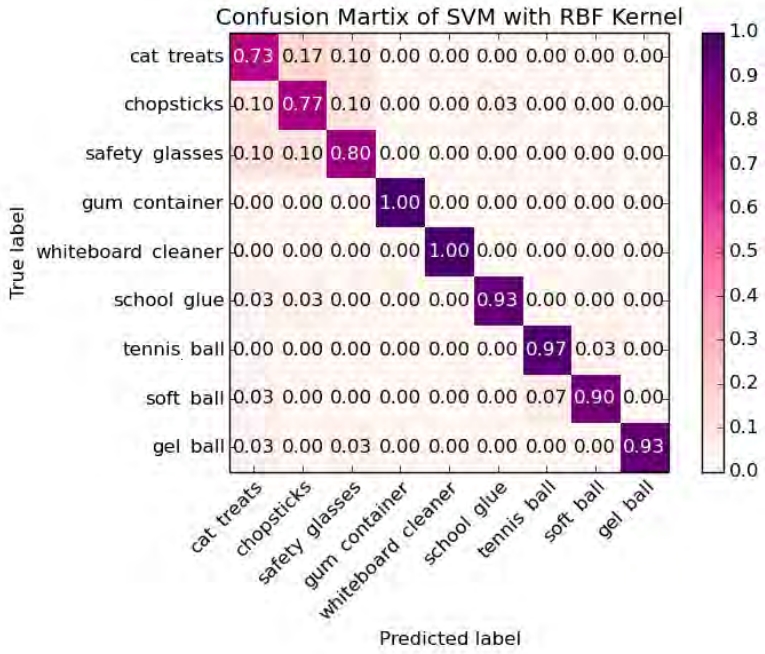

Figure 5.7: This confusion matrix shows the classification rate of the object set based on tactile sensor data.

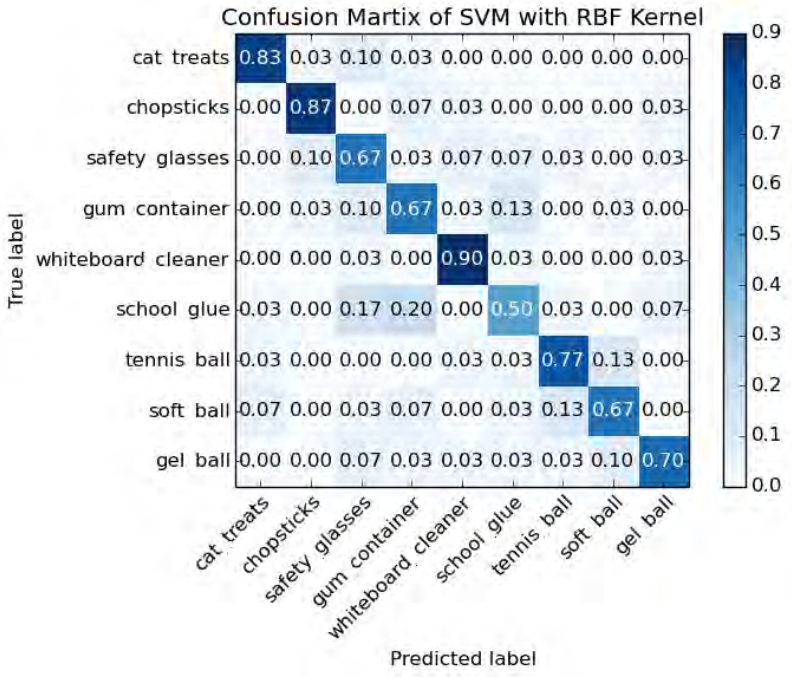

Figure 5.8: This confusion matrix shows the classification rate of the object set based on air pressure sensor data.

the whiteboard cleaner even reach 100% accuracy. These two objects belong to the object group of plastic bottles, they have rigid bodies and symmetrical footprints. This could suggest that these shapes are well recognizable for the tactile sensor.
The confusion matrix for the air pressure sensor in shown in figure 5.8. Compared to the tactile sensor, no specific object group stands out with a particular high or low prediction accuracy, but the overall accuracy is lower. Except for two objects: Even though the overall prediction accuracy of the air pressure sensor is lower, the prediction accuracy for the cat treats and the the chopsticks is higher with 83% and 87%, compared to 73% and 77% for the tactile sensor. Since these two objects belong to the same object group, this suggest that the performance of the classifier differs among the object groups.

5.3 Prediction Analysis

When we selected the objects set, we segmented it in three object groups, each group with it's individual features (see Sec. 5.1). The three groups are different from each other in many attributes, but inside the groups the objects are quite similar. We now take closer look at how the predictions differ among the groups.
Therefore we separate the classification results we computed previously in three section, separated by their object groups: How many objects are predicted correctly, How many objects are predicted incorrectly, and how many are predicted incorrectly but were still placed inside the correct object group? This way we can compare how the groups perform next to each other. Fig. 5.9 presents the prediction analysis for both sensor types. For the plastic bottle, the tactile sensor achieves the highest classification rate across all groups and sensor. The objects in this group have a rigid body in common. From the confusion matrix we know that the gum container and the whiteboard cleaner even scored a 100% prediction accuracy. These two have a circular footprint in common, while the third object in this group, the school glue, has a oval shape. The balls also have symmetrical shapes, but can deform due to their softness. The prediction accuracy in this group is slightly lower compared to the plastic bottles. This suggest that the tactile sensor performs best with rigid, symmetrical shapes. Based on the tactile sensor, the objects in packaging have the lowest prediction accuracy among the three groups. But the objects that are labelled incorrectly by the classifier are almost all placed inside the correct object group.
This is not the case for the predictions based on the air pressure sensor. With this sensor, the objects in packaging are recognized with a slightly higher accuracy than with the tactile sensor. But among the incorrect labels among, approximately half of

baby

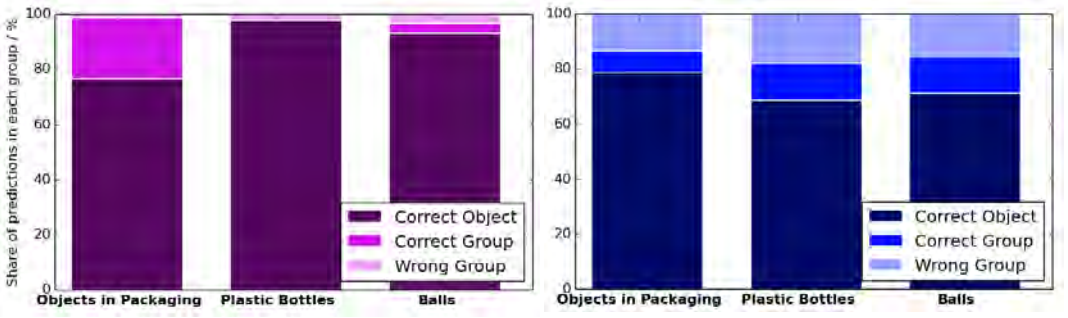

a) tactile sensor b) air pressure sensor

Figure 5.9: Prediction analysis for the tactile sensor array (a) and the air pressure sensor (b). The classification rates are displayed proportionally to the number of objects in their group.

the objects in packaging were placed in the wrong group. The same pattern applies to the other two object groups, the plastic bottles and the balls. Here the prediction accuracy is not only lower compared to the tactile sensor, but approximately half of the labels are outside of the group, too.

Overall we summerize that the tacile sensor performs better for most objects, and even for wrong labels it can still correctly predict the correct object group. The reason why the sensor performs worse for objects in packaging could lie in the movement of the objects inside their packaging. While these objects are grasped, the objects are shifted and the object is deformed. But unlike the soft balls, they don't return to their previous shape after the grasp is released. Instead, the objects slightly change their shape with every grasp.

5.4 Spatial Resolution

The sensor is intentionally designed with a high spatial resolution with the aim to increase the amount of information we extract from the environment. Compared to the air pressure sensors, which only receive two values per finger, the tactile sensor delivers 14 dimensional data information per finger. So far we have demonstrated that the tactile sensor achieves higher classification accuracies compared to the air pressure sensor. In this section we investigate if the superior classification rate of the tactile sensor is a result of its higher spatial resolution.

We compare the performance of sensors with different spatial resolutions. To get tactile sensor data with lower resolutions we artificially reduce the spatial resolu-

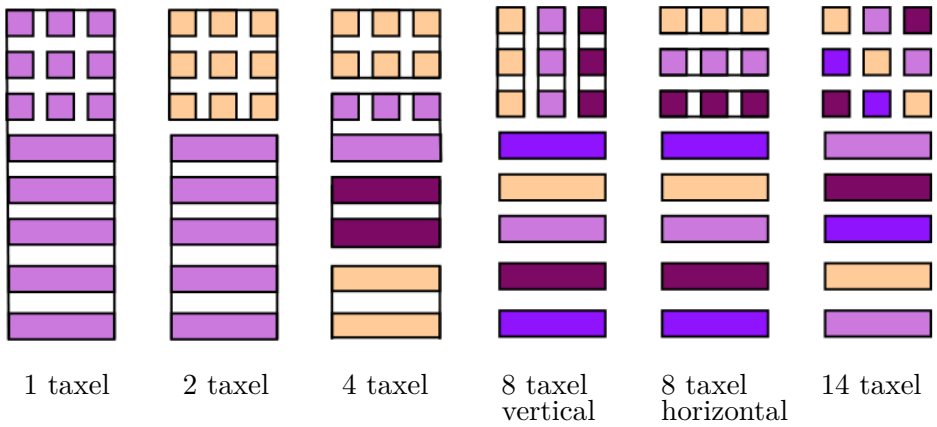

Figure 5.10: We simulate 6 different spatial resolutions for the tactile sensor by merging group of taxels. Taxels marked with the same color are combined to form a new, larger taxel. From left to right: One singel taxel by computing the average of all taxel values. Two taxels by merging the small taxels at the fingertip to one taxel and the larger taxels below to a second taxel. Four taxels by merging all taxels in four equally sized areas. Eight taxels by merging the small taxels at the finger tip to three vertical stripes. Eight taxels by merging the small taxels at the finger tip to three horizontal stripes. And finally the original 14 taxels resolution by not merging any taxels.

tion of the existing data. This has the advantage that the results are comparable, since the predictions for all resolutions will be based on the same data set. The resolution of the air pressure sensor is also artificially reduced from two to one air compartments per actuator. This simulates an PneuFlex actuator with only one air compartment.
To investigate the other side of the spectrum, we also maximize the spatial resolution. By combining the two sensory modality of tactile and air pressure sensors, we maximize the available sensor data and draw from the benefits of both sensor types. For each sensor resolution we generate, we compute the prediction accuracy by leave-one-out cross-validation, as already explained more detailed in chapter 5.2. Then we observe how the changed resolutions affect the prediction accuracy.

To reduce the spatial resolution of the tactile sensor, we select a group of taxels and compute the average of their sensory output. With this method, we can simulate different resolutions on the existing data set. All resolutions we explore for the tactile sensor are visualized in figure 5.10. Next to the original 14 taxel of the sensor, we simulate tactile sensors with one, two, four and eight taxel. For the eight taxel, we try merging the small taxels at the finger tip in two different ways: Once by merging them in vertical lines, and once in horizontal lines.

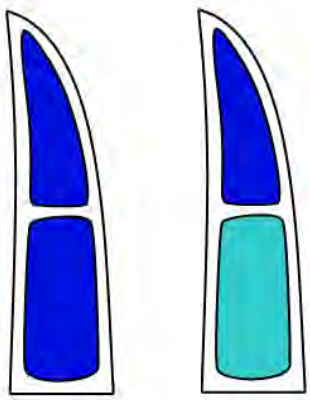

Figure 5.11: This figure shows the cross-section of the PneuPlex actuator with two air compartments. For each compartment, we have an air pressure value. To simulate a PneuPlex actuator with only one air compartment, we compute the average of the two air pressure values.

The four sensorized fingers of the gripper have two air compartments each. To reduce the spatial resolution of the air pressure sensors, we compute the average of the top and bottom air compartment. This way, we simulate a RBO Hand 2 with one-compartment PneuFlex actuators. Figure 5.11 shows the cross-section of the PneuFlex actuator with two air compartments on the right side and the simulated actuator with one compartment on the left side.
The maximal spatial resolution is achieved by adding the two sensory modalities of tactile and air pressure sensors. We concatenate two data points, the 56 dimensions of the tactile sensor arrays and the 8 dimensions of the air pressure sensors, to create a new 64 dimensional datapoint that contains both sensory outputs. Up to this point we only used the air pressure information of the four fingers that are equipped with tactile sensors. To further maximize the information density, we also test the classification with all 11 dimensions of the air pressure data. Together with the tactile sensor, this gives us a $56 + 11 = 67$ data point. To distinguish the combined data, we will mark the results based on the full air pressure data with an additional "+".
All together we have 10 sensor resolutions to compare: six tactile resolutions (1, 2, 4, 8v, 8h, 14), two air compartment resolutions (1, 2) and two combinations of both sensors (14+2 and 14+2+). For each resolution, we optimize the hyperparameters before we train the SVM classifier. This way we ensure that we provide the best prediction accuracy for each resolution.

The classification rate for each resolution is displayed in Fig. 5.12. The tactile

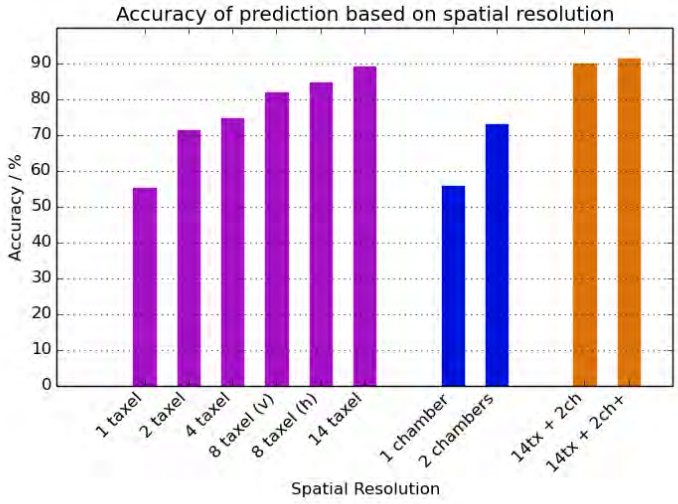

Figure 5.12: This bar plot shows the classification rate of different sensor resolutions of the tactile sensor, the air pressure sensor and the combination of both.

sensor with only one taxel per finger reaches with 55.2% approximately the same prediction accuracy as the one-compartment actuator with 56%. Similar, two taxel per sensor reach a similar accuracy as the two-compartment actuator with 71.5% and 73%, respectively. From there the classification rate increases with increasing number of taxels. For 8 taxel, the rate is with 84.8% slightly higher if the taxels at the finger tip are merged in horizontal stripes, compared to 81.9% with the vertical stripes. With the full 14 taxels of the sensor we achieve the accuracy of 89.3% like we did in pervious chapters.
For the combination of both sensors, in Fig. 5.12 highlighted in orange, we achieve even higher classification rates. With all taxels and the air pressure of 4 fingers (14tx+2ch), we achieve 90% classification accuracy, exceeded only by the tactile sensor with all air pressure information (14tx+2ch+) at 91.5%.

In conclusion we can say that tactile sensing alone is not superior than the air pressure sensors, as they produce the same prediction accuracies at the same resolution. But with increasing spatial resolution the tactile sensor can draw more information from its environment and provide predictions with higher accuracy.

6 Conclusion and Outlook

In the beginning of this work we discussed the requirements we want our tactile sensor array to meet. We wanted our sensor to be flexible and provide continuous measurement at a high spatial resolution. We looked at a variety of approaches to soft tactile sensing and highlighted their advantages and disadvantages. We also examined the available option to realize a high spatial resolution and manage the cabling that comes with it.
The sensor we propose in this work is made from from EeonTex piezoresistive fabric, a flexible nylon fabric with a large range of resistivity based on the applied pressure. The high spatial resolution of 14 taxel is realized with a flexible PCB which we custom designed to fit out actuator. This allowed to keep the sensor, and therefore later the actuator, free of cables as they were attached at sensor part located at the base of the actuator.
We found a characteristic line that describes the relationship between sensor in- and output. This characteristic lines defines the sensitivity and measuring range of the tactile sensor. With different resistors in the sensor reading setup we can influence the characteristic line to fit the needs of our application.

With the help of a silicone sleeve we integrated the tactile sensor array to four fingers of the RBO Hand 2. By testing two different mounting orientations, we found the orientation that minimizes the influence of the actuation of the Pneu-Flex actuator on the sensor output. We also investigated the influence of the sensor array on the actuator: Comparing the compliance of a sensorized actuator to an unsensorized actuator showed that the proposed tactile sensor does not restrict the compliant behavior of the actuator significantly.

With the sensorized RBO Hand 2 we grasped 9 different object from 3 object groups. During the grasps, we gathered sensory information from four tactile sensors on the hand as well as the air pressure sensors of the actuator air compartments. We successfully performed object classification based on both sensory information and found that the tactile sensor achieves higher prediction accuracies overall. Even in the case of a incorrect prediction, the tactile sensor is able to match an object to the correct object group. Based on the classification results of each object group we identified which object features that enable or hinder a high recognition rate by the

tactile sensor. We learned that the classification based on the tactile sensor favours symmetrical objects that remain constant in their shape over time. We also learned that rigid object are easier recognizable compared to soft objects.
To investigate the significance of the high spatial resolution for the prediction accuracy of the tactile sensor, we tested several alternative resolution. This revealed that the superior prediction accuracy is only based on the spatial resolution of the sensor. When reduced to the same resolutions, the classification of the tactile sensor and air pressure sensor perform the same.

This works proposed a sensor that is first of its kind for the RBO Hand 2. It offers a solid foundation to continue the development of improved sensors in the future. We demonstrated the importance of the spatial resolution for classification results. A next step could be to even increase the resolution even more.
Since we only sensorized four fingers of the RBO Hand 2 there is also the option to sensorize the remaining actuators of the hand. Tactile sensors in various shapes and resolutions can be applied to the palm and the thumb to increase the spatial resolution.
All experiments on the RBO Hand that are included in this work were conducted with the hand fixed on the table top by its wrist. The tactile RBO Hand 2 at its current state can not be mounted to a robot arm because the reading setup of the tactile sensors, two breadboards and four Labjack U6, are too large and heavy to fit in the limited space by a robot. To use the tactile sensor in a more dynamic environment, new data reading solution have to be found that ideally reduce the complete reading setup to the size of a micro-controller.
Towards the end of this work we introduced the idea to combine the tactile sensor information with information from an other sensor. With more sophisticated sensor fusion techniques than the one we applied, the combination of two or more sensors on the RBO Hand 2 could be further exploited and improve object classification rates.

Bibliography

[1] Mohsen Kaboli, Armando T. De La Rosa, Rich Walker, and Gordon Cheng. In-hand object recognition via texture properties with robotic hands, artificial skin, and novel tactile descriptors. *IEEE-RAS International Conference on Humanoid Robots*, 2015-Decem:1155–1160, 2015. ISSN 21640580. doi: 10.1109/HUMANOIDS.2015.7363508.

[2] Alexander Schneider, Jürgen Sturm, Cyrill Stachniss, Marco Reisert, Hans Burkhardt, and Wolfram Burgard. Object identification with tactile sensors using bag-of-features. *2009 IEEE/RSJ International Conference on Intelligent Robots and Systems, IROS 2009*, pages 243–248, 2009. doi: 10.1109/IROS.2009.5354648.

[3] Nicholas Farrow, Lauren McIntire, and Nikolaus Correll. Functionalized textiles for interactive soft robotics. *Proceedings - IEEE International Conference on Robotics and Automation*, pages 5525–5531, 2017. ISSN 10504729. doi: 10.1109/ICRA.2017.7989651.

[4] Ozgur Atalay, Asli Atalay, Joshua Gafford, and Conor Walsh. A Highly Sensitive Capacitive-Based Soft Pressure Sensor Based on a Conductive Fabric and a Microporous Dielectric Layer. *Advanced Materials Technologies*, 3(1):1–8, 2018. ISSN 2365709X. doi: 10.1002/admt.201700237.

[5] Van Ho and Shinichi Hirai. Design and Analysis of a Soft-Fingered Hand With Contact Feedback. *IEEE Robotics and Automation Letters*, 2(2):491–498, 2017. ISSN 23773766. doi: 10.1109/LRA.2016.2645120.

[6] Raphael Deimel. Soft Robotic Hands For Compliant Grasping. *Doctoral dissertation*, 2017.

[7] Zhanat Kappassov, Juan Antonio, Corrales Ramon, and Véronique Perdereau. Tactile sensing in dexterous robot hands - Review. *Robotics and Autonomous Systems*, (June 2018), 2015. doi: 10.1016/j.robot.2015.07.015.

[8] K. Weiss and H. Worn. The working principle of resistive tactile sensor cells. *IEEE International Conference Mechatronics and Automation, 2005*, (July): 471–476, 2005. ISSN 0022-3727. doi: 10.1109/ICMA.2005.1626593.

[9] Hongbo Wang, Massimo Totaro, and Lucia Beccai. Toward Perceptive Soft Robots: Progress and Challenges. *Advanced Science*, 5(9), 2018. ISSN 21983844. doi: 10.1002/advs.201800541.

[10] Hanna Yousef, Mehdi Boukallel, and Kaspar Althoefer. Tactile sensing for dexterous in-hand manipulation in robotics - A review. *Sensors and Actuators, A: Physical*, 167(2):171–187, 2011. ISSN 09244247. doi: 10.1016/j.sna.2011.02.038.

[11] Yong Lae Park, Bor Rong Chen, and Robert J. Wood. Design and fabrication of soft artificial skin using embedded microchannels and liquid conductors. *IEEE Sensors Journal*, 12(8):2711–2718, 2012. ISSN 1530437X. doi: 10.1109/JSEN.2012.2200790.

[12] John Morrow, Hee Sup Shin, Calder Phillips-Grafflin, Sung Hwan Jang, Jacob Torrey, Riley Larkins, Steven Dang, Yong Lae Park, and Dmitry Berenson. Improving Soft Pneumatic Actuator fingers through integration of soft sensors, position and force control, and rigid fingernails, 2016. ISSN 10504729.

[13] Xi Fang, Zemin Liu, Yufei Hao, Hui Yang, Jiaqi Liu, Zhexin Xie, and Li Wen. A Soft Actuator with Tunable Mechanical Configurations for Object Grasping Based on Sensory Feedback. *2019 2nd IEEE International Conference on Soft Robotics (RoboSoft)*, pages 25–30, 2019.

[14] Harish Devaraj, Kartik Yellapantula, Mathilda Stratta, Andrew McDaid, and Kean Aw. Embedded piezoresistive pressure sensitive pillars from piezoresistive carbon black composites towards a soft large-strain compressive load sensor. *Sensors and Actuators A: Physical*, 285:645–651, 2019. ISSN 09244247. doi: 10.1016/j.sna.2018.12.006.

[15] Marc Antoine Lacasse, Vincent Duchaine, and Clément Gosselin. Characterization of the electrical resistance of carbon-black-filled silicone: Application to a flexible and stretchable robot skin. *Proceedings - IEEE International Conference on Robotics and Automation*, (June 2015):4842–4848, 2010. ISSN 10504729. doi: 10.1109/ROBOT.2010.5509283.

[16] Sravan Salibindla, Brice Ripoche, Daniel T.H. Lai, and Simon Maas. Characterization of a new flexible pressure sensor for body sensor networks. *Proceedings of the 2013 IEEE 8th International Conference on Intelligent Sensors, Sensor Networks and Information Processing: Sensing the Future, ISSNIP 2013*, 1: 27–31, 2013. doi: 10.1109/ISSNIP.2013.6529758.

[17] Jawad Mehmood Butt, Hesheng Wang, and Radan Pathan. Design, Fabrication, and Analysis of a Sensorized Soft Robotic Gripper. *8th Annual IEEE International Conference on Cyber Technology in Automation, Control and Intelligent Systems, CYBER 2018*, pages 169–174, 2019. doi: 10.1109/CYBER.2018.8688201.

[18] Gereon H. Büscher, Risto Kõiva, Carsten Schürmann, Robert Haschke, and Helge J. Ritter. Flexible and stretchable fabric-based tactile sensor. *Robotics and Autonomous Systems*, 63(P3):244–252, 2015. ISSN 09218890. doi: 10.1016/j.robot.2014.09.007.

[19] Godwin Ponraj, Senthil Kumar Kirthika, Nitish V. Thakor, Chen Hua Yeow, Sunil L. Kukreja, and Hongliang Ren. Development of flexible fabric based tactile sensor for closed loop control of soft robotic actuator. *IEEE International Conference on Automation Science and Engineering*, 2017-Augus:1451–1456, 2018. ISSN 21618089. doi: 10.1109/COASE.2017.8256308.

[20] J. H. Low, W. W. Lee, P. M. Khin, S. L. Kukreja, H. L. Ren, N. V. Thakor, and C. H. Yeow. A compliant modular robotic hand with fabric force sensor for multiple versatile grasping modes. *Proceedings of the IEEE RAS and EMBS International Conference on Biomedical Robotics and Biomechatronics*, 2016-July:1230–1235, 2016. ISSN 21551774. doi: 10.1109/BIOROB.2016.7523799.

[21] Diliang Chen, Yi Cai, and Ming Chun Huang. Customizable pressure sensor array: Design and evaluation. *IEEE Sensors Journal*, 18(15):6337–6344, 2018. ISSN 1530437X. doi: 10.1109/JSEN.2018.2832129.

[22] Roland S. Johansson and J. Randall Flanagan. Coding and use of tactile signals from the fingertips in object manipulation tasks. *Nature Reviews Neuroscience*, 10(5):345–359, 2009. ISSN 1471003X. doi: 10.1038/nrn2621.

[23] R. S. Johansson and A. B. Vallbo. Tactile sensibility in the human hand: relative and absolute densities of four types of mechanoreceptive units in glabrous skin. *The Journal of Physiology*, 286(1):283–300, 1979. ISSN 14697793. doi: 10.1113/jphysiol.1979.sp012619.

[24] Raphael Deimel and Oliver Brock. A compliant hand based on a novel pneumatic actuator. *Proceedings - IEEE International Conference on Robotics and Automation*, pages 2047–2053, 2013. ISSN 10504729. doi: 10.1109/ICRA.2013.6630851.

[25] Gereon H. Büscher, Risto Koiva, Carsten Schurmann, Robert Haschke, and Helge J. Ritter. Tactile dataglove with fabric-based sensors. *IEEE-RAS International Conference on Humanoid Robots*, pages 204–209, 2012. ISSN 21640572. doi: 10.1109/HUMANOIDS.2012.6651521.

Internet

[26] `http://www.robotics.tu-berlin.de` (Last accessed: 2016-04-18)

A Appendix: Construction Manual

A.1 Tactile Sensor

A.1.1 List of Components

The following lists specify all materials that are necessary to build one tactile sensor:

FlexPCB	A custom made flexible printed circuit board. The documentation and the Gerber files for the manufacuring can be found in the Git project "soma_flexpcb" in the RBO Lab repository.
Piezoresistive Fabric	The fabic used so far is EeonTex™ LTT-SLPA by Eeonyx, there are other fabrics with similar properties by the same manufacturer. The piece of fabric should at least be $20mm \times 80mm$ to cover all taxels.
Conductive Fabric	Any highly conductive fabric is sufficient, usually they are made from silver covered nylon fabric. The piece needs to be at least $20mm \times 100mm$ to cover the whole sensor plus an overhang to attach the grounding cable.
Adhesive Tape	Minimum width of $50mm$, length of $200mm$. The thinner the tape the better.
Cables	15 cables of $15 - 25cm$ length, 14 for the taxels plus one cable for grounding.
Pin Strip Headers	15 pins are necessary, 14 for taxel outputs plus one pin for grounding
Spiral Cable Wrap	Length should be approximately be the same as the cables

To process the materials, you need the following tools:

- Laser Cutter
- Soldering station
- Pliers to cut and strip the cables
- Hot glue gun
- Scissors

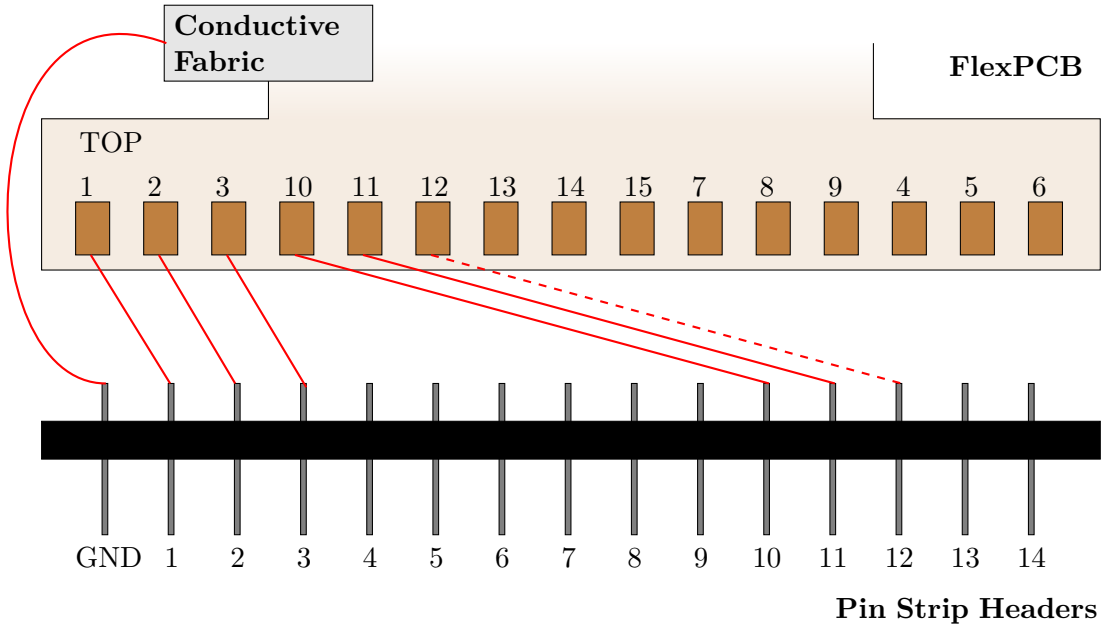

Figure A.1: This chart demonstrates how each taxel output of the flexPCB (top) is connected to the pin strip headers, the taxel output and the pin with the same number must be connected. The cables are marked in red, note that just a few exemplary cables are shown to keep the chart overseeable.

- Optional: Ohmmeter instrument

A.1.2 Step-by-Step Instructions

1. Prepare the Adhesive Tape Layers
   a) the adhesive tape is cut from double sided adhesive tape by a laser cutter. The Adobe Illustrator file (*.ai) for the cutting pattern is located at Git project "soma_flexpcb" in the RBO Lab repository.
   b) To place the tape inside the laser cutter, stick it onto a second piece of tape to ensure the top layers stays clean from burn marks of the laser cutter. Later, use only the top clean layer of tape.
   c) Cut with the following settings:
   [VECTOR : Speed=100% Power=10% Frequency=100%]
   d) Repeat the process for a second tape layer. One is required between the flexPCB and the piezoresistive fabric and a second one for between the piezoresistive and the conductive fabric.
2. Assemble the Layers of the Sensor

a) Take the custom flexPCB and position it so that the big exposed copper pads that will make the taxels are on the top. Make sure the surface is free from oil and dust.

b) Place the first layer of adhesive tape on the flexPCB in a way that the holes of the tape are alined with the exposed copper pads of the sensor. Press the tape on the sensor, then remove the cover sheet of the tape.

c) Place the layer of piezoresistive fabric on top of the adhesive tape and press it on. Make sure the complete sensing area is covered by the material. Avoid any stretching and wrinkling of the material, because it changes the conductive properties of the material.

d) Cut around the shape of the flexPCB to remove the overhanging fabric.

e) Place the second layer of double sided adhesive tape on top of the piezoresistive fabric. This time, the location of the taxels is not visible. Align the tape as good as possible with the outline of the flexPCB, press it on and remove the cover sheet of the tape.

f) Place the conductive layer on top of the adhesive tape. Create a $1cm$ overhang on the side of the wiring, and press it on.

g) Cut around the shape of the flexPCB to remove the overhanging fabric EXCEPT on the side of the wiring.

3. Attach the Cables to the FlexPCB

a) Flip the sensor so the conductive fabric is facing down. At the end of the flexPCB are 15 exposed copper pads to attach cables to. Make sure the exposed copper pads are free from oil and dust.

b) Cut 15 pieces of cable at $15 - 25mm$ length, depending on how long you want the connection between sensor and the analog-digital converter to be.

c) Take 14 cables, strip $1 - 2mm$ of the insulation off and solder one cable each to the copper plates 1-14 of the flecPCB as shown in Figure A.1. Note that the indices of the copper pads are not consecutive and copper pad 15 (in the middle) is currently not used.

d) Take the last cable and strip the top $10mm$ of the insulation off. Attach the cable to the conductive fabric on the overlap we left before. The easiest way to do it is by piercing the fabric several times with the cable and then bending the cable so that it can not slip back out of the fabric.

e) OPTIONAL: To check if there is no electrical short between any of the sensor output, connect two neighbouring output cables to a ohmmeter instrument. The resistance between these cables should be infinitely high. If that's not the case, check if there is any soldering tin residues that connects the two outputs at the soldering spots. Repeat with all neighbouring cable pairs.

4. Connect the Pin Strip Headers

   a) Cut all cables coming from the sensor to the same length. Strip ca $10mm$ of the insulation off the cables.

   b) Solder the cables to the pin strip in the order shown in figure A.1. Note that the order of the copper pads and therefore the cables is not consecutive.

   c) The pin stripe will be the hardware interface of the sensor.

5. Isolate Soldering Points with Hot Glue Gun

   a) The hot-melt adhesive from the hot glue gun is used to insulate the soldering spots and protect them from breaking.

   b) Apply liquid adhesive onto the soldering spots on the flexPCB. Make sure all soldering tin and all uninsulated cables are covered, and that no uninsulated cables are in contact with each other creating a short.

   c) Apply liquid adhesive onto the side of the pin strip with the cables. Make sure all soldering tin and all uninsulated cables are covered, and that no uninsulated cables are in contact with each other creating a short.

A.2 Sleeve to Attach the Sensor to the Actuator

A.2.1 List of Components

Acrylic Glass	The glass needs to be $3mm$ thick, and should not be smaller than $5cm \times 15cm$
Acrylic Glass Glue	
Double Sided Adhesive Tape	
Silicone	Dragon Skin 10
Silicon Glue	
Crepe Tape	Minimum width of $50mm$
OPTIONAL: Silicone Pigments	Special pigments to dye silicon, any color

To process the materials, you need the following tools:

- Laser cutter
- File and sandpaper
- scale, plastic cup and spatula for the silicone

A.2.2 Step-by-Step Instructions

1. Create the cast
   a) Cut the casting mold for the sleeve from the acrylic glass. It is formed like the contour of the sensor, a vector graphic file for the laser cutter can be found in the Git project "soma_flexpcb" in the RBO Lab repository.
   b) Use the file and sandpaper to radius and smooth all edges of the mold. The silicon will later be too thin and ruptured at places where it stretched over hard edges.
   c) Fixate the mold vertically on a small even surface, eg. a piece of acrylic glass or a piece of wood, so it can stand vertically by itself.
2. Cast the sleeve
   a) Prepare the Dragon Skin 10, for just one mold mix $3g$ of each mixing components, for two molds $5g$ of each mixing component.
   b) Cover the surface of the mold evenly with the silicone. Make sure there are no holes in the surface.
   c) Let the silicone cure by letting it stand vertically. You will see that the silicon layer will be slightly thicker at the bottom after curing. This is due to gravity making the silicon run downwards

d) Prepare a second round of Dragon Skin 10, with the same amount as before. Again, cover the whole surface of the mold. This time, let the silicone cure while hanging the mold upside down. By this, we make the silicon run to the other side of the sleeve during the curing process and compensate the irregularity of the first silicon layer.

3. Add the sleeve to the tactile sensor

   a) Cut a piece of double sided adhesive tape in the shape of the sensor using the laser cutter. A vector graphic file with all needed cutting lies can be found in the Git project "soma_flexpcb" in the RBO Lab repository. Place the adhesive tape on the side of the backside of the flexPCB and press it on.

   b) Remove excess silicon at the base and the tip of the silicon sleeve with scissors or a cutter. Roll the sleeve upwards starting at the base, rolling towards the tip.

   c) Remove the cover sheet of the adhesive tape, then place the sleeve on the tip of the sensor and roll the sleeve down. The adhesive tape will prevent the sensor from moving inside the sleeve.

4. OPTIONAL: mark the taxel locations on the sleeve.
   For some tasks or experiment it is important to know where the taxels are located on the sensor.

   a) Cut a mask for the color from crepe tape using the laser cutter. A vector graphic file with all necessary cutting lines can be found in the Git project "soma_flexpcb" in the RBO Lab repository

   b) Place the mask on the sleeve of the senor, on the side where the grey conductive fabric is visible through the sleeve. Make sure to align the mask well with the contour of the senor to make sure that the holes in the mask are aligned with the taxels on the flexPCB below. This can be tricky as the tape does not stick well to the silicon surface of the sleeve.

   c) Give a hazelnut sized amount of silicon glue on a clean surface. Then add some silicon coloring pigments and mix the glue with a spatula until the glue has a consistent color. In the example I used black pigments because it gives a good contrast to the grey below, but any other color works as well.

   d) Use the spatula to smear the colored silicon glue across the mask in a thin layer. Make sure the mask does not move during the process.

e) Let the glue dry and remove the mask. Now the colored rectangles and squares should be placed on the sleeve where the taxels are on the sensor.

5. Attach sensor to actuator

a) Apply a thin layer of silicon glue to the side of the sleeve where the flexPCB is visible through the sleeve.

b) Gently place the sensor on the actuator, the bottom of the sensor where the cables are attached should face the base of the actuator, the side of the sensor with the small and dense taxels go on the finger tip of the actuator.

c) To ensure that the sensor does not move and stays pressed to the actuator, I suggest wrapping the actuator and sensor with crepe tape from top to bottom, like a soft cast, until the glue is cured.

d) Once the glue is dry, remove the wrapped tape and enjoy your new tactile actuator!